CIAMTIS

U.S. DOT Region 3 University Transportation Center

Multi-robot teaming for inspection of hydraulic structures

June 14, 2024

Prepared by:

D. Lattanzi, K. Aminfar, George Mason University; M. Head, S. Safari, University of Delaware;

r3utc.psu.edu

PennState College of Engineering

LARSON TRANSPORTATION INSTITUTE

DISCLAIMER

Technical Report Documentation Page

1. Report No. CIAM-UTC-REG51	2. Government Accession No.	3. Recipient's Catalog No.
Multi-robot teaming for inspection of hydraulic structures: Final Report		5. Report Date June 14, 2024
		6. Performing Organization Code
7. Author(s) David Lattanzi, Kiyarash Aminfar, Monique Head, Sajjad Safari		8. Performing Organization Report No.
9. Performing Organization Name and Address Center for Infrastructure Public-Private Partnership Policy Schar School of Policy and Government George Mason University 3351 Fairfax Dr., MS 3B1 Arlington, VA 22201		10. Work Unit No. (TRAIS)
		11. Contract or Grant No. [Enter contract number here]
12. Sponsoring Agency Name and Address U.S. Department of Transportation Research and Innovative Technology Administration 3rd Fl, East Bldg E33-461 1200 New Jersey Ave, SE Washington, DC 20590		13. Type of Report and Period Covered Draft Final Report 07/01/2022 – 12/31/2023
		14. Sponsoring Agency Code
15. Supplementary Notes		

16. Abstract

Inspecting hydraulic structures, including capturing deformations in the deck and detecting defects in the piers, presents numerous challenges. These structures require evaluation both above and below the water surface, and existing approaches do not support quantitative and integrated asset management practices. This study develops a multimodal computer vision framework that utilizes a combination of Digital Image Correlation (DIC), robotic imaging, and photogrammetric analysis to improve the inspection of hydraulic structures. The framework was experimentally evaluated under laboratory and field conditions. The team used the laboratory experiments to understand key environmental variables that impact computational imaging in a marine scenario. The field experiments were performed on the Route 1 bridge spanning the Occoquan River in Woodbridge, Virginia. The team used the field tests to better understand the impacts of logistical constraints, to evaluated how laboratory scale processes scaled to full scale infrastructure, and to demonstrate potential for integration with conventional assessment methods. A robot-human teaming approach is utilized to gather visual imagery for both above and below-water surfaces. To overcome the difficulties of underwater imaging, artificial lighting is employed, as well as image enhancement methods designed specifically for marine environments. How environmental variables present in the marine environment impact data quality and potential data products was exhaustively explored. To capture the dynamic response of the bridge, the study utilizes a DIC non-contact measurement system to monitor deck deflections and estimate its dynamic characteristics such as natural frequencies and mode shapes. The results from the DIC systems were used to inform the calibration process and create a digital twin Finite Element (FE) model. The findings and methodologies of the technology integration have significant potential applications in infrastructure maintenance, such as bridge maintenance and dam safety. The project includes partnership and dissemination with partnering Departments of Transportation (DOT), namely the Virginia Department of Transportation (VDOT) and the Delaware Department of Transportation (DelDOT).

17. Key Words Computer vision, Structure-from-Motion (SfM), Photogrammetry, Submerged infrastructure, Underwater inspection, Marine robots, Bridge inspection	18. Distribution Statement No restrictions. This document is available from the National Technical Information Service, Springfield, VA 22161

19. Security Classif. (of this report) Unclassified	20. Security Classif. (of this page) Unclassified	21. No. of Pages 43	22. Price

Form DOT F 1700.7 (8-72) Reproduction of completed page authorized

Table of Contents

Table of Figures

CHAPTER 1

Introduction

BACKGROUND

Many transportation structures have components located in waterways, such as coastal marine environments or riverine systems. The most common of these components are the substructures of bridges spanning waterways. As with all bridges in the United States, DOTs are legally obligated to inspect and maintain these bridge components on a routine basis, per the National Bridge Inspection Standards (NBIS) put forth by the Federal Highway Administration (FHWA) [1].

These bridge substructure components, referred to here as hydraulic structures, pose unique challenges for DOTs and inspection engineers since they require complex rigging operations and specialized dive teams during the inspection (Figure 1).

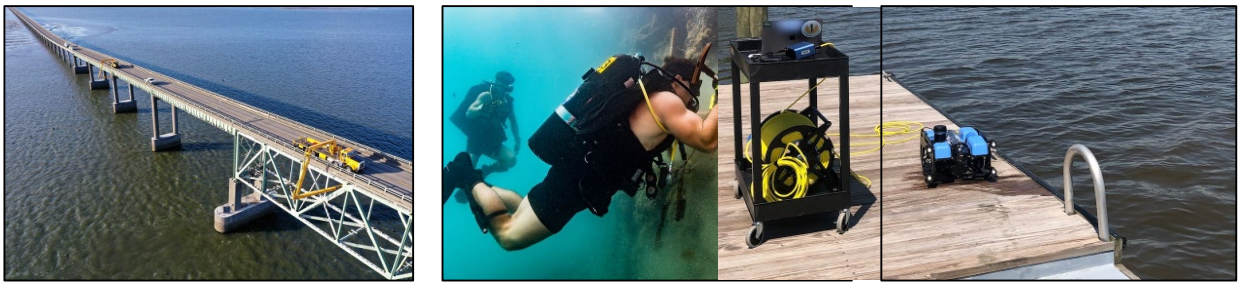

Figure 1. Hydraulic bridge and snooper truck [2], inspection dive team [3], and inspection ROV.

So-called "snooper trucks" supported from the bridge deck are expensive and cause significant traffic disruptions. Climbing teams can mitigate traffic disruptions but are costly to deploy and not always widely available. Often, hydraulic structural inspections also require the use of expensive temporary platforms within a waterway that can disrupt traffic through a waterway.

These challenges are compounded by the fact that, by their nature, these structures are partially submerged in a given waterway. The submerged portions of the structures are subjected to complex hydraulic loadings that accelerate degradation or destabilize the structure. Most notably is the scour phenomenon, in which water channel flows cause concentrated erosion around bridge foundations, ultimately leading to collapse.

Given the challenges of inspecting these structures, they are excellent candidates for the use of robotics. Several commercial companies offer robotic inspection services. However, current capabilities remain limited with respect to quantitative and automated data analysis, mechanistic understanding of collected data and, critically, with the systematic connection of robotically collected data with element-level NBIS inspection protocols. Robotic inspection systems have been deployed above the waterline [4–7], as well as below [8–12]. However, few studies simultaneously combine data from above and below the water for

integrated assessment. Relevant studies have considered data fusion of sonar and imaging for reconstruction[13–16], or using multi-robot teams in a post-disaster context [17,18].

OBJECTIVES

The objective of this research project is to advance the state of the art in monitoring hydraulic structures through the development of a multi-modal inspection framework that includes digital imaging information from both humans and robots. This framework is designed to collect digital images of the structure above and below the water surface separately. The complete set of information from the team is then assessed through machine learning and computer vision methods that provide automated and quantitative assessment data. Analyzing the complete set of information allows for automated, element-level bridge inspection and holistic assessment of the complete hydraulic structure.

Specific objectives of the project include:

- An evaluation of existing robotic and sensor technologies and inspection protocols
- A study of robotic approaches to imaging underwater structural components
- A study of approaches for imaging above water components
- Experimental testing of these approaches under laboratory and field conditions

The project advances the state of the art in condition assessment through the development of robotic, computer vision, and artificial intelligence methods to automate data collection and analysis, and by directly integrating that data with existing asset management practices. The project includes laboratory experiments and a series of full-scale field experiments on the Route 1 Bridge over the Occoquan River in Woodbridge, Virginia.

DATA AND DATA STRUCTURES

The digital images collected in both the laboratory and field experimental tests, and products generated from these digital images, are the primary data for this project. These digital images include both still images and video recordings from an array of cameras. In addition, a variety of programming scripts were generated for the purposes of processing and analyzing all project data. The project also resulted in the creation of numerical finite element models used for experimental validation and digital twin integration.

CHAPTER 2

Existing approaches and protocols

REMOTE SENSING FOR STRUCTURAL INSPECTION

Engineers rely on measurements for designing, constructing, and maintaining infrastructure to meet stringent standards for quality, safety, and performance. Advanced technologies are continuing to emerge to assist with bridge inspections. These technologies, including sensors, 3D scanning [19,20], photogrammetry [21–23], LiDAR (Light Detection and Ranging) and Digital Image Correlation [24,25], machine learning and Artificial Intelligence (AI) [26,27] have played a crucial role in advancing measurement capabilities in structural engineering.

Vision-based measurements offer several advantages, including the ability to capture measurements in multiple locations within the field of view. This method allows the use of different cameras for various purposes, ensuring easy and quick deployment. The ability to "re-test" by replaying videos is another notable advantage, along with non-destructive measurement that minimizes disturbance to traffic and geopolitical considerations compared to conventional methods. Engineers can effectively utilize this measurement technique as a reliable and relatively low-cost approach for assessing structures. Furthermore, they can update models and create digital twins by calibrating them based on captured measurements.

Digital imaging technology has transformed remote structural monitoring, allowing non-contact monitoring of structures and infrastructures that pose challenges for traditional sensor arrays [28,29]. This includes large-scale composite structures, the wind energy and aerospace sectors, difficult-to-access locations such as bridges, and culverts [20,29–32]. Additionally, digital imaging offers optical flow for measuring displacements, enabling the visualization of magnified versions of small displacements and precise structural vibration measurements [20,33].

Reagan et al. [34] devised an innovative method for non-contact, optically based measurements for health monitoring of bridges in challenging or hazardous locations. They combined the use of an unmanned aerial vehicle and three-dimensional digital image correlation. Baqersad et al. [21] reviewed the application of various photogrammetry techniques (including DIC) in structural dynamics, comparing them with other measurement techniques such as laser Doppler vibrometry and interferometry techniques. Displacement measurements of a large-scale scaled model of a structure were monitored via a low-cost 360° panoramic camera-based measurement, with nodes in images automatically located and tracked by a proposed deep learning-based algorithm [35].

UNDERWATER INSPECTION AND DATA ANALYSIS

For the inspection of underwater components, the focus was on robotic methods, particularly those that use digital imaging as a sensor payload. The choice of robotics was based on conversations with DOT partners and an assessment of the challenges associated with human dive team inspections.

Underwater robotic inspection

For the purposes of this report, the term robot is used to refer to autonomous, semi-autonomous, and remotely piloted systems including Remotely Operated Vehicles (ROVs), and Unmanned Surface Vehicles (USVs). The integration of robotic systems significantly enhances the capabilities of infrastructure inspection and monitoring in both above water and underwater environments [36–39]. For a thorough understanding of the application of the robotic systems in infrastructure monitoring the reader is directed to [40,41]. In particular, examining the above-water segments of structures using robots has been a frequent topic of study [42–44]. Utilizing multiple teams of robots requires considerations such as autonomy in navigation and different levels of collaboration between robots or human operators [45]. In one study, the authors proposed a framework for a team of robots split into two roles: certain robots approach the structure collecting detailed information (proximal observers) while the rest (distal observers) keep a distance providing an overview of the mission and assist in the localization of the proximal observers [46]. Combining the efforts of human operators with robots that are used to capture images in more hazardous or hard-to-reach locations is a widely employed method in inspection [38,47,48] that facilitates comprehensive data collection. This collaborative approach improves the quality and quantity of data acquired. Overall, the literature review points to a major need for many more studies on applications for submersible robots. The lack of studies on underwater robotic systems is largely due to challenges with underwater imaging, scene understanding, and analysis.

Underwater imaging and image analysis

The underwater environment poses substantial challenges for scene understanding. These challenges are predominantly due to the intrinsic variability of aquatic settings, characterized by factors such as depth of water [49], and light [50]. The interaction of light with water involves scattering and absorption, referred to as attenuation [49]. Environmental factors like the existence of particulates in water [51,52] and fluctuating underwater light conditions (flicker) [53], can significantly undermine image quality in underwater scenes and also can alter color consistency and contrast [52,54]. Environmental conditions can culminate in detail loss and color alteration [55]. Variability in luminance conditions and other material attributes of underwater environments can further distort color uniformity and contrast [52]. Camera-related elements like lens distortion and chromatic aberration [56], as well as experiment-specific metrics like camera-to-structure distance and surface texture and reflectivity, also contribute to these variances. Several underwater image enhancement methods have been proposed, including filter based methods [57,58], color correction based methods [59,60], image fusion based methods [61] as well as fusion of multiple data sources, like optical and sonar image fusion [62,63], or acoustic and stereo camera fusion [64].

Recently, the landscape of underwater imaging technology has witnessed substantial advancements across various areas, including image enhancement and restoration techniques [49,54,61,65,66]. Comparing image restoration techniques with image enhancement, the latter is simpler because it does not require additional prior knowledge about the water parameters. Underwater image enhancement techniques include, but are not limited to, contrast enhancement, non-uniform illumination correction, and color correction techniques [49].

Depth estimation is a popular topic, given its influence on understanding the underwater scene. A method employing an unsupervised network for depth estimation and color correction from monocular images addresses the issue of model generalization [67]. Studies also include obtaining a simple yet fast binary representation of the foreground and background depth map of the underwater scene with low-level image features [59], deriving inherent optical properties from background colors [68], and a depth estimation method based on image blurriness and light absorption [52]. The exploration of depth estimation based on water classification using monocular images marks a significant advancement in robotic underwater perception [69].

The creation of specialized datasets tailored to underwater environments is crucial as these resources enable the training and testing of machine learning models on data that reflect the complexities of these settings [50,61,70]. However, it is important to note that despite the notable successes of deep learning, its demands for extensive datasets and complex tuning can be challenging, and are often excessively complex [71]. Consequently, techniques that do not require extensive labeled datasets or complex tuning, such as techniques applied on a single image, are an important subset of approaches.

In underwater imaging, images are often unlabeled and originate from diverse global locations with varying visibility conditions. These images, captured by different individuals, present unique challenges due to the absence of standard references for water type and environmental conditions [49]. Direct measurement of water quality parameters like turbidity or light penetration using instruments is often very challenging. As a result, metrics derived from images are often used. The diverse distortions, including chroma decreasing, low contrast, nonuniform illumination, blurring, non-uniform color casting, and noise from complicated factors present in underwater images make it hard to establish a universal image quality metric for all types of underwater environments [61]. Among different quality assessment metrics, the Underwater Color Image Quality Evaluation (UCIQE) metric [72] significantly contributes to evaluating and understanding underwater image quality and color distortion along with many other image quality metrics such as the Color Image Quality Index (CIQI) [73]. In addition, there exist revised metrics like Color Quality Enhancement (CQE) [74], which linearly combines different metrics for colorfulness, sharpness, and contrast. Introduction of the Simulated Water Type Dataset (SWTD) based on Jerlov water types furthers this effort by providing a platform for underwater image quality analysis [75].

The categorization and analysis of images based on their similarity are essential for many analysis applications such as content-based image annotation and image retrieval. For instance, consider applications where scene-specific image processing is necessary [50]. This allows for targeted monitoring of areas prone to rapid degradation, improving the management and prioritization of maintenance activities [70]. Consequently, engineers can more precisely evaluate structural issues like wear, corrosion, or biofouling, enabling timely interventions that prevent failures and ensure adherence to environmental and safety standards.

The problem of creating a 3D reconstruction of solely underwater portion of the structure or the above water portion have been studied extensively and the reader is directed to [76–78] for additional comparison between different techniques and their key features. A major research area is on generating comprehensive 3D reconstructions of submerged infrastructure. Although there have been attempts to achieve this using tools such as multi beam sonar [79], or combinations of sonar and laser data [80,81], limited work has been reported employing SfM. The influence of focal length on 3d measurement is investigated for underwater scenes in [82]. Linking below and above water 3D reconstructions using installed targets and a stereo rig capturing data from both medium simultaneously was considered in [83].

DIGITAL IMAGE CORRELATION IN BRIDGE MONITORING

Vision-based measurements utilizing DIC have significantly improved engineering, particularly in structural analysis. They provide non-contact methods for capturing deformations and movements in structures and objects [84], marking a shift from visual inspections to more reliable monitoring systems [85]. DIC achieves this by numerically correlating a selected subset of the digitized intensity pattern of the undeformed object, enabling the acquisition of full-field deformations [86]. Monitoring data related to deflection or displacement of structures under various loads, including seismic or vibrations, involves capturing the relative motions of points (pixels in a region of interest) in the video recording [86]. DIC systems are exemplified by Imetrum Dynamic Monitoring System (DMS) [87], the commercial system used for this research project.

The wide adoption of full-field and non-contact measurement in DIC has piqued interest in large-scale composite structure testing, wind energy, and aerospace sectors for displacement and strain measurements under static loading and operational modal analysis in dynamic structural tests. This is due to the advantages of DIC over conventional point-wise measurement techniques [32]. DIC has demonstrated capabilities in non-contact target tracking of bridges (e.g., pedestrian bridges) under seismic and dynamic loads, suggesting its potential for larger structural health monitoring applications [22]. Vibration measurements and model updating techniques provide the potential to optimize the structural performance of various structures under diverse operational and environmental conditions using different approaches, whether deterministic or probabilistic.

CHAPTER 3

Robotic imaging for underwater structural inspections

INTRODUCTION

The literature review covered in Chapter 2 highlighted the fact that underwater robotic imaging has not seen widespread adoption as an inspection technology, particularly relative to more established technologies such as sonar. There are two primary reasons for this. The underwater environment is highly variable with respect to imaging conditions, and the impacts of those conditions on image quality are not well understood. Additionally, there is a lack of methods designed to characterize the quality and nature of the underwater images themselves. This characterization is important for downstream analysis tasks such as image processing and defect detection, algorithmic tasks that are difficult to generalize across broadly varying underwater environments. Chapter 3 covers the studies undertaken in response to this assessment.

ROBOTIC INSPECTION METHODOLOGY

The goal of this work was to capture images in underwater scenes and use them to create 3D reconstructions, following the approach illustrated in Figure 2. This comprehensive pipeline, inspired by the workflow described in reference [88], includes dataset collection and preparation and a 3D reconstruction pipeline.

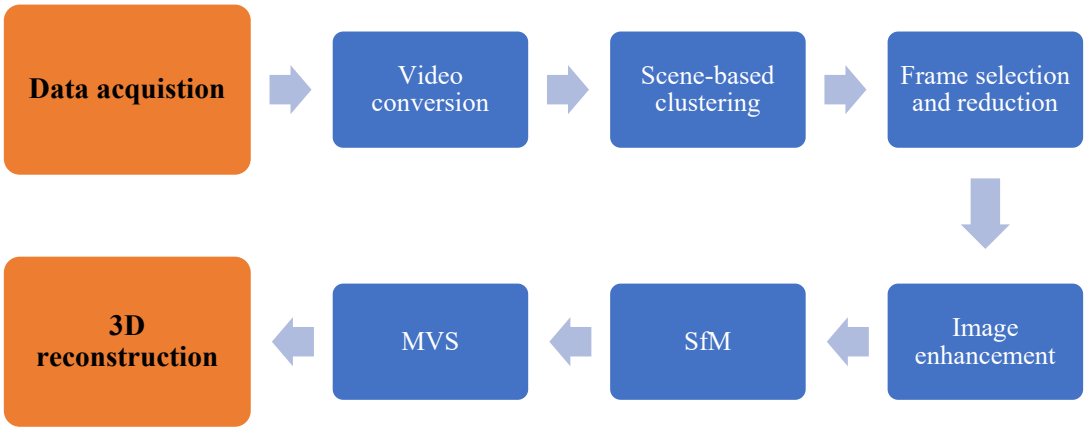

Figure 2. Robotic inspection framework.

Image preprocessing

Regardless of the imaging modality, images in this work are acquired in the form of videos. Key frames are extracted from these videos based on a similar approach introduced in [89]. These frames are then further reduced to minimize computational efficiency based on the clustering approaches discussed in [90].

To improve image quality, WaterGAN [91], an unsupervised generative model recognized for its efficacy in enhancing and color-correcting underwater images was utilized here. WaterGAN's architecture is adept at addressing the non-uniform color shifts and varying degrees of blurring and light absorption often present in underwater imaging, making it particularly suited for the heterogeneous conditions of underwater scenes. Its generative approach facilitates the reconstruction of lost details and the correction of color casts, thereby significantly improving the fidelity of underwater imagery.

3D scene reconstruction

SfM is primarily used to recover the 3D positions of camera viewpoints and a sparse set of 3D points from a sequence of images. It involves identifying key points across multiple images, matching these points between images, and then using these correspondences to infer both the 3D position of the points and the pose (position and orientation) of the camera when each photo was taken. The output is typically a sparse 3D point cloud, as it focuses on significant features in the image. This sparse point cloud is further processed to create a dense point cloud. The details of the SfM process are not included here, for brevity. For an in-depth exploration of optical methods in 3D reconstruction, readers are referred to [78]. A rigorous parameter sensitivity study was undertaken to optimize the quality and robustness of generated point clouds.

After obtaining the 3D point cloud, manual refinement and the application of more robust techniques are needed to eliminate outliers and smooth the point cloud. As demonstrated in the author's previous work [92,93], kriging has proven beneficial, leading to a better alignment of points within the grid, an anticipated advantage when registering above and below water point clouds.

Registration, scaling, and camera calibration

In 3D modeling and image processing, registration, scaling, and calibration are critical processes that enhance the accuracy and utility of data [94]. Point cloud registration employs algorithms such as the Iterative Closest Point (ICP) to align multiple point cloud datasets into a single coordinate system, effectively minimizing discrepancies across different captures. This process often utilizes reference objects known as calibration targets, which are placed in the scene to provide fixed reference points.

Inspired by other researches [82], a custom target system was designed and manufactured using two cast acrylic sheets (Figure 3). In the target the following features were included: Connection holes, aligned holes, ruler-like indentations, rectangular circular and star-shaped carvings, and a unique grid pattern. Each feature supported the pattern recognition capabilities of the algorithm.

Two calibration targets were assembled and mounted on an aluminum beam, allowing for the system to be placed in such a way that one board would be submerged and the other above water. Adjacent to each target board, color calibration boards were placed, ensuring accurate color correction. The target system facilitates registration by providing a diverse array of distinct, easily recognizable features. The high-contrast features also supported camera calibration by providing multiple high quality points for feature detection. This aids in the determination of camera distortions and the calculation of both intrinsic and extrinsic parameters, which are essential for accurate 3D reconstruction. The known dimensions of the scale bars provide a measurable scale within the imaging field. The calibration targets were used to correct lens distortions and improve the fidelity of color in images. and ensuring that the imagery from different cameras can be integrated seamlessly.

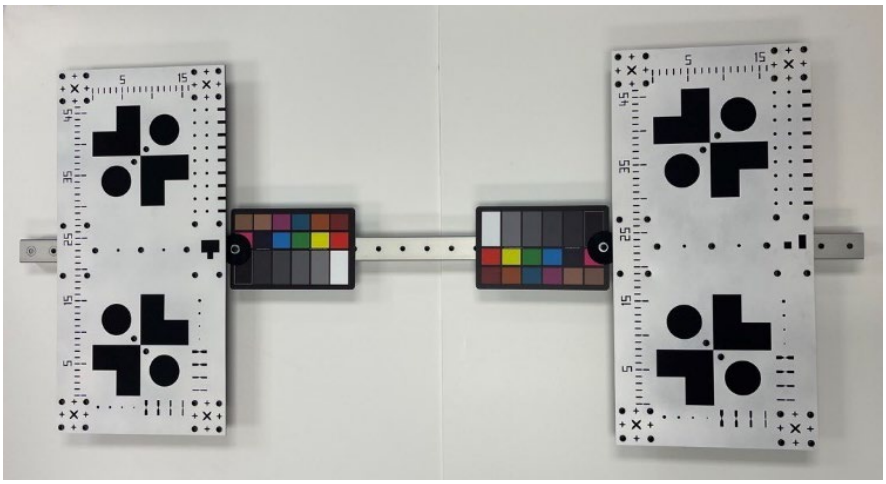

Figure 3. The custom targets and color boards used in this study, with geometric patterns and color chart.

Evaluation metrics for 3D reconstructions

To assess the quality of the 3D reconstructions generated in this study, various evaluation metrics were employed. One of the metrics used to evaluate the quality of 3D reconstructions is the percentage increase in matched photos and extracted features. A higher percentage increase in matched photos and extracted features typically results in a more accurate and complete 3D reconstruction.

Reprojection error is a widely used metric for evaluating the accuracy of 3D reconstructions. It measures the average discrepancy between the observed 2D image points and the projected 2D image points obtained by reprojecting the reconstructed 3D points back onto the image plane. Lower reprojection errors indicate a more accurate reconstruction.

Point cloud density is a measure of the spatial distribution of points within the point cloud. It is an essential metric for evaluating the level of detail in a 3D reconstruction. Higher point cloud density generally leads to more detailed and accurate representations of the underlying structure, which is crucial for effective damage assessment and structural health monitoring.

Completeness is a metric that quantifies the extent to which a 3D reconstruction covers the entire structure of interest. A high level of completeness ensures that all parts of the submerged infrastructure are represented in the 3D model, critical for a comprehensive assessment of structural integrity. Completeness can be assessed by comparing the reconstructed model with ground truth data or expert annotations, where available

Another common approach is to use reference points on the 3D calibration target as check points for accuracy assessment. The RMSE between the reconstructed coordinates and the known coordinates of check points can then be calculated [95].

STUDY 1: EXPERIMENTAL ANALYSIS OF ROBOTIC IMAGING

Laboratory Testing

The laboratory experiments were conducted in a circular water tank. A bracing system was designed to maintain the specimen centrally suspended in the water column at a predetermined height from the tank's

base. The specimen was attached to an inverted turntable via a connecting rod, enabling controlled rotational movements within the aquatic medium (Figure 4).

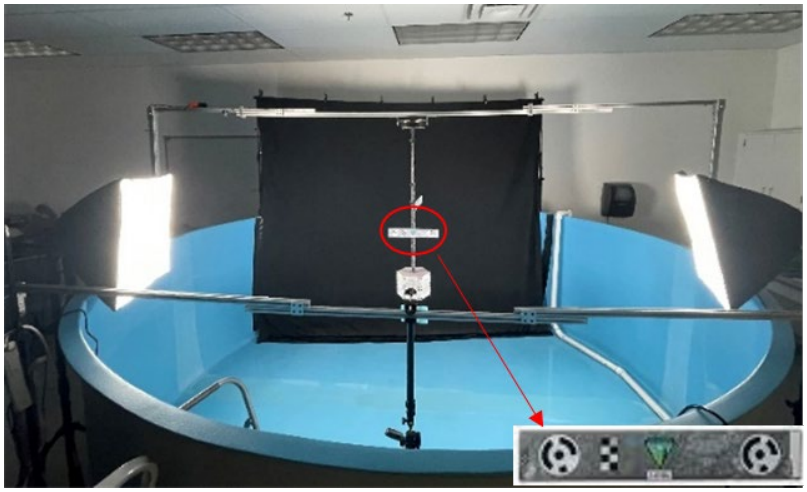

Figure 4. Lab experimental setup.

Imaging and lighting

For the above-water imaging, an Olympus TG-6 camera was mounted on a retractable rod that utilized a bracing system analogous to that of the specimen. This arrangement facilitated precise positioning and movement of the camera, mirroring the dynamics experienced in actual field conditions. The camera was positioned at a specified distance from the specimen to optimize the field of view and image clarity, thereby increasing the efficiency of the data collection process. In parallel, for the underwater imaging, a GoPro camera equipped with an underwater housing was deployed. This setup ensured coverage of the underwater portion of the specimen along the above water at the same time, aligning with the experimental objectives.

The lighting environment was controlled using a combination of artificial light sources including photography light stands, soft boxes, and umbrellas used as light modifiers. These tools were employed to achieve a range of lighting conditions categorized into three levels: low, medium, and high intensity. The intensity was regulated by the number of active light bulbs, with their distribution carefully adjusted to maintain symmetrical lighting relative to the specimen's location. Light intensity measurements were taken using a light meter. Although the use of light modifiers slightly reduced the intensity, they were critical in diffusing the light to produce uniform and homogeneous illumination of the specimen, considering the camera's viewing angles.

The artificial lighting was intended to mimic natural sunlight conditions typically encountered in field settings. Additionally, three sets of specialized LED lights were integrated into the camera rig to enhance the illumination of the underwater parts of the specimen, ensuring that all visible surfaces were adequately lit for high-quality imaging.

Turbidity modeling

There are a variety of methods used to simulate the optical conditions commonly encountered in natural underwater environments and that typically degrade image quality. These conditions include reduced visibility, color distortion, and scattering effects, all of which pose significant challenges in underwater imaging. This work focused on water turbidity, a common challenge in marine environments. To simulate turbidity, Kaolin clay was added to the water tank in increments, as shown in Table 1. As a baseline, the specimen was also imaged in an empty tank (case 0).

Table 1. Created turbidity via added Kaolin clay.

Case #	Kaolin weight (g)
1	0
2	7
3	14
4	21
5	28

Test specimens

A novel 3D specimen was designed to simulate various defect types and sizes (Figure 5). The specimen was designed as a hexagon with six flat vertical surfaces, each serving as a canvas for artificial defects. This shape was chosen because it allows for equal distribution and clear visibility of defects. Defects were designed to emulate both material removal (indentation) and addition (extruded volume), mimicking real-world damage scenarios such as cracks, bulging, swelling or other kinds of visible deformations. Half circle shapes were applied on sides 1 (indentation) and 4 (additional volume). Triangle shapes were applied on sides 2 (indentation) and 5 (additional volume). Rectangle shapes were applied on sides 3 (indentation) and 6 (additional volume).

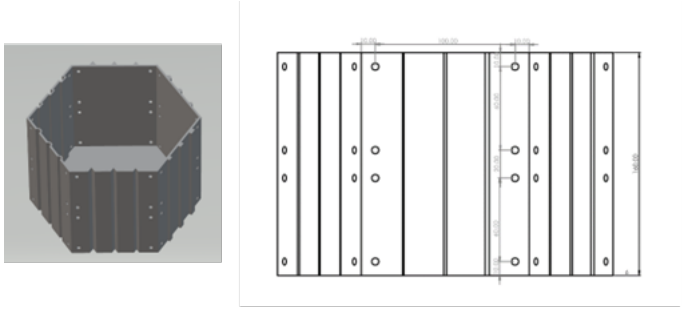

Figure 5. Specimen model and sketch.

Given the reliance of photogrammetry for reconstruction, the initially texture-less 3D prints were modified to enhance feature recognition. To this end, the surfaces of each specimen were speckled with red, green, and blue paint. This not only facilitated the photogrammetry process by enhancing surface detail visibility but also allowed for the examination of color degradation effects in underwater conditions.

Laboratory experimental results

The 3D reconstructions generated using the SfM pipeline are shown in Figure 6. In all the cases the distance between the camera and the target is 1 m. As the turbidity increases, the uncertainty in the point cloud is increases due to the inherent noise in the scene. The added noise in Case 5 (highest turbidity) results in the reconstructed surface no longer being a flat surface. The images for Case 5 were then enhanced using WaterGAN and the results is shown in Figure 7. Although the 3D reconstruction is significantly improved, it is still dramatically degraded.

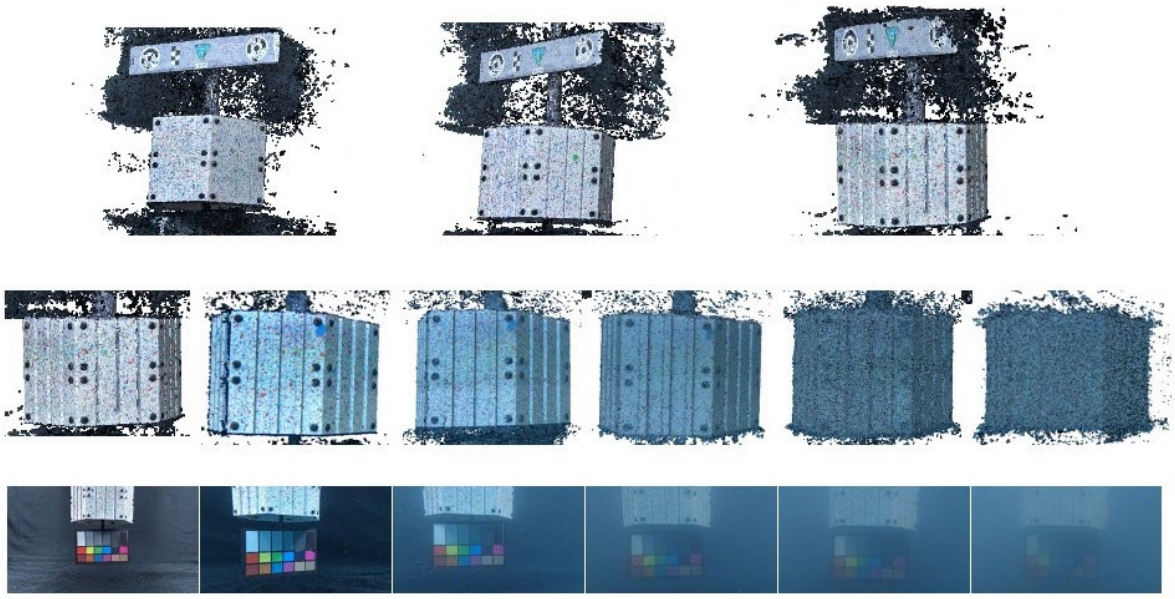

Figure 6. 3D reconstructions under laboratory conditions, for increasing levels of water turbidity (from left to right). Far left case is for an empty tank (Case 0).

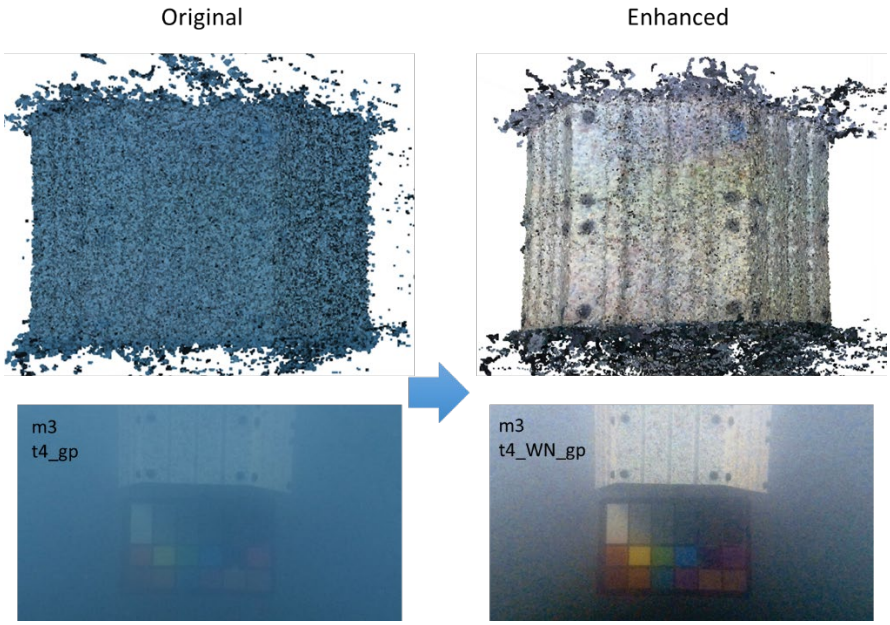

Figure 7. Visual representation of Waternet enhancement in the highest turbidity condition (Case 5): 3D reconstruction and representative images.

Field Testing

Full-scale field testing of the 3D reconstruction process was also undertaken. In this study, a robot-human collaborative strategy was employed for data acquisition [45]. The teaming strategy combined the efforts of human and Remotely Operated Vehicles (ROVs) to capture images in challenging underwater environments. The main subject of the study was a pier of a bridge located in Occoquan, VA. The pier number 3 and 4 as depicted in Figure 8 was the main target of data acquisition. During tests

Figure 8. Occoquan bridge and target piers shown by red rectangles.

Data acquisition

For underwater imaging, both a robotic and manual imaging system were tested. The manual system included a GoPro camera fitted with an underwater housing and a specialized underwater Wi-Fi transmitter, accompanied by additional lighting to optimize visibility (Figure 9). Although in underwater environment the absorption of light components varies with the depth, in close-range capture this problem can be solved by using artificial light sources as strobes or lamps [55]. An ROV camera operated at a resolution of 1920 x 1080 pixels, balancing image quality with data manageability. Additionally, the TG-6 camera, utilized for capturing videos from above water, also recorded at a resolution of 1920 x 1080 pixels.

Figure 9. Underwater manual imaging system.

The data acquisition process was conducted under various test conditions over 3 days that presented a range of challenges for image capture and 3D reconstruction. Factors such as water turbidity, light conditions, and water currents impacted the operation and consequently the image quality and the resulting 3D reconstructions (Figure 10).

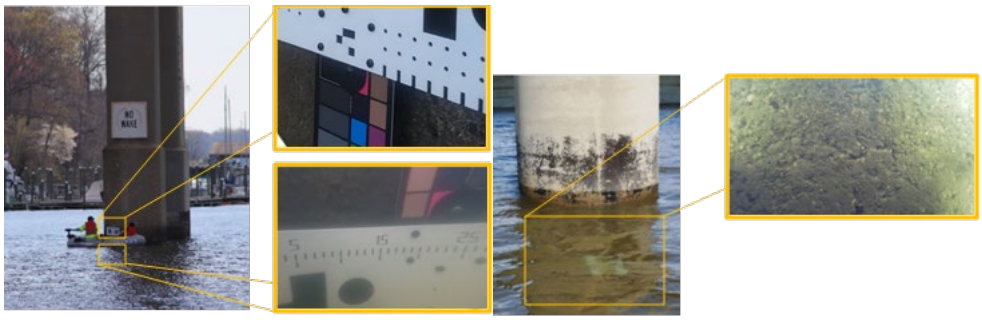

Figure 10 An overall view of the bridge pier, and the acquired images from underwater and above water portion of the pier.

Field experimental results

A sensitivity analysis of the SfM parameters was conducted for the underwater dataset (Table 2). The results for a subset of dataset are visualized in Figure 11, showing different combinations of parameters and the difference they make in the 3D reconstruction.

Table 2. The configuration of parameters in Model A, B, and C.

Case name	Model A	Model B	Model C
Camera model	Pinhole	Radial	Radial
Estimate affine shape	No	No	Yes
Guided matching	No	No	Yes
Compute relative pose	No	Yes	Yes
Ba global use pba	No	Yes	Yes

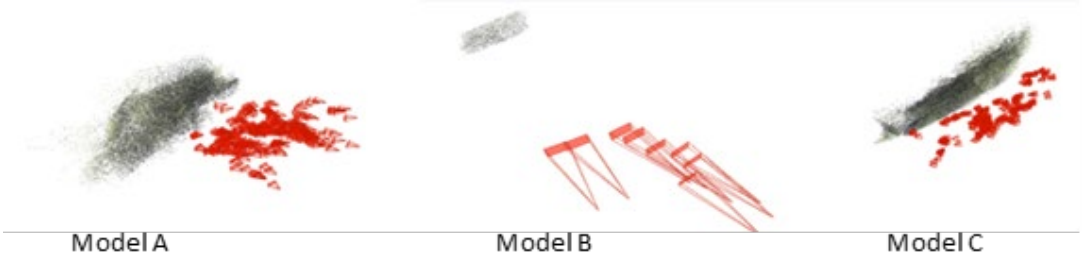

Figure 11. Visual comparison of parameter study for model A, B, and C.

As depicted in Figure 12 and Figure 13, guided matching emerged as a crucial factor in enhancing the point cloud's quality and exerted a significant influence on the overall results. In addition, considering variable parameters in the case of close-range underwater infrastructure monitoring, additional constraints such as considering the scene as planar and estimating affine shape throughout the process can prove beneficial. This is particularly true for scenarios involving the condition assessment of large infrastructures like piers, ships, dams, and the like, where the scene is typically planar.

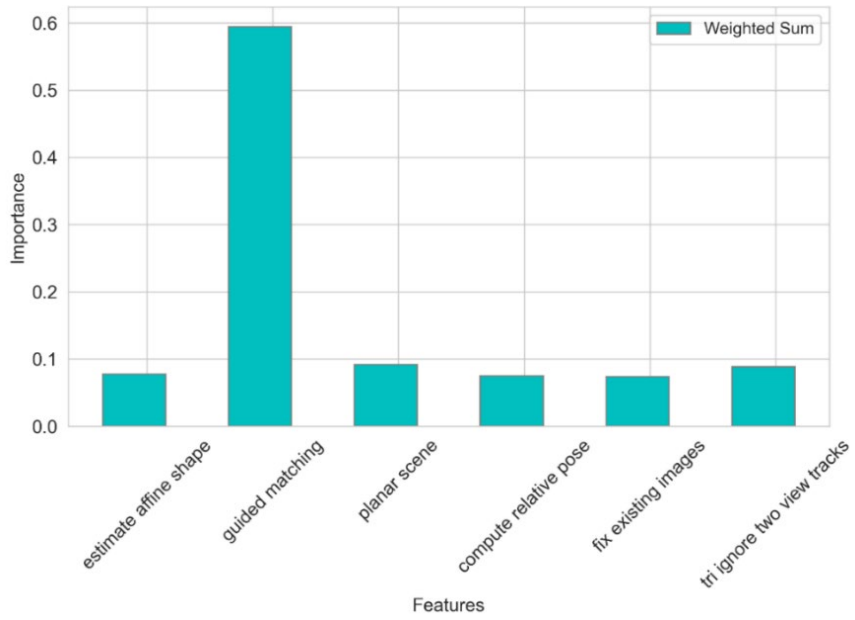

Figure 12. Relative importance of binary hyperparameters in the reconstruction process

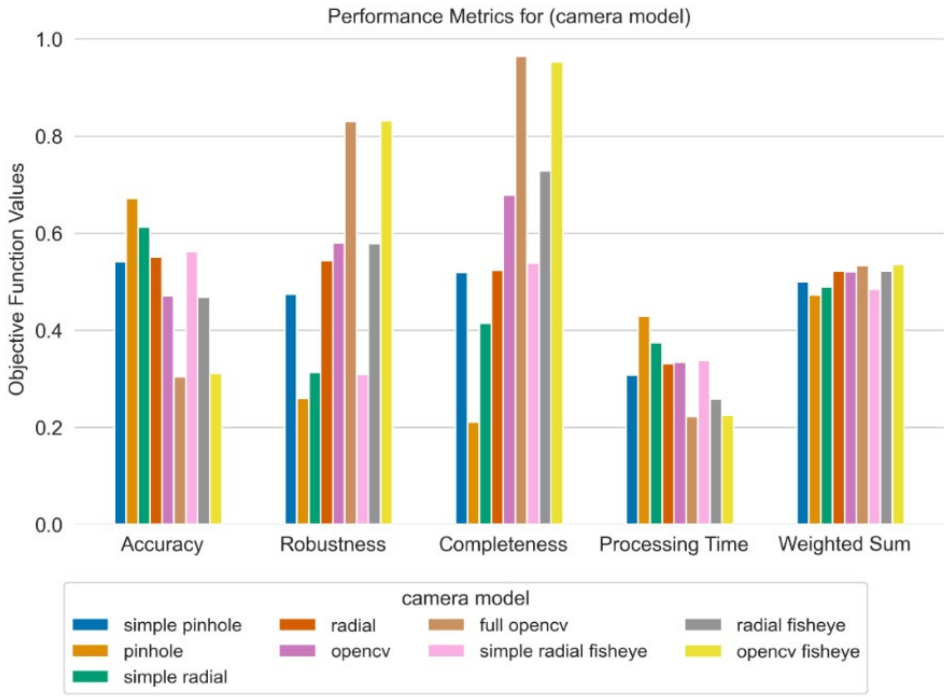

Figure 13. Comparative performance metrics for 3D reconstructions.

As confirmed in the lab tests, the turbidity observed during field testing was too high for successful 3D reconstruction. The usage of image enhancement techniques proved to be useful in the visual appeal and detection of defects (Figure 14), but it was not able to overcome the low light and turbid conditions. The amount of murkiness in the field test riverine environment was more than the highest turbidity scenario model in the lab. The conclusion is that additional advancements are necessary before 3D reconstructions can be viable under similar field conditions.

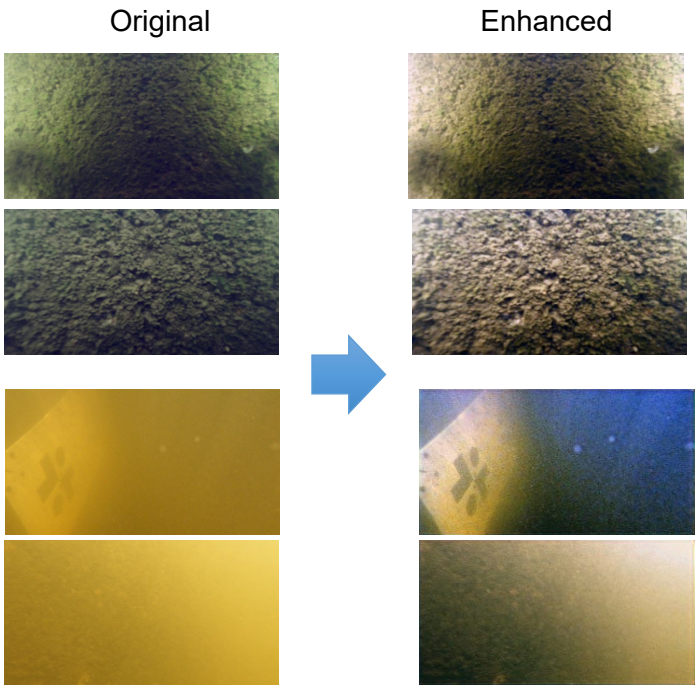

Figure 14. Underwater infrastructure images before and after Waternet enhancement.

Findings and Conclusions

This research aimed to develop a pipeline for condition assessment of submerged infrastructure using Structure-from-Motion (SfM), clustering and machine learning techniques, combined with robot-human collaboration for data acquisition. GAN-based image enhancement techniques improved the quality of underwater images, leading to better input data for the SfM pipeline. The SfM pipeline in the laboratory environment proved to be effective. The robot-human collaborative strategy proved to be effective in capturing underwater images under field conditions. However, turbidity, water currents, and visibility changed throughout the tests, which affected image quality. The high levels of turbidity and low light in the testing environment made SfM reconstruction extremely difficult and only limited reconstructions were possible.

Recommendations For Future Studies

The enhancement techniques applied in this study significantly improved image quality. However, several potential improvements were identified:

- Adaptive enhancement techniques: Future research could investigate adaptive enhancement techniques that can adjust their parameters based on the characteristics of each image, resulting in better overall image processing performance.
- Integration of deep learning: Deep learning-based image enhancement methods have shown promising results in underwater imaging. Investigating such methods could lead to improvements in image quality.

- Use of other data sources: Fusing sonar data or employing laser scanner could help. However, the cost associated with these methods should be considered.
- Scour detection: the poor visibility at the marine bed is challenging for divers and robots alike. Most of the conventional robots use propeller thrust to navigate. This potentially leads to shifting debris, algae and other disturbances that reduces the visibility and increase turbidity. Alternative robotic systems that do not cause such disturbances should be studied.

STUDY 2: ANALYSIS METHODS FOR CATEGORIZING AND CLUSTERING UNDERWATER IMAGES

While recent advancements in underwater image analysis across fields such as object detection, image enhancement, and image restoration are notable, the challenges posed by unlabeled and no-reference images from diverse global locations and varied visibility conditions remain significant. Unlike conventional approaches that focus primarily on objects within images, this study emphasizes analyzing inherent image features to enhance understanding and interpretation in the absence of reference data.

This research introduces a novel pipeline designed for categorizing and clustering underwater images based on intrinsic scene characteristics, specifically targeting characteristics associated with visibility, color, texture, and content, ultimately capturing the water type condition. This approach is particularly pertinent as it shifts the analytical focus from object-based to environment-based understanding, which is critical in diverse aquatic conditions.

The study is structured around three primary objectives:

- Development of robust preprocessing and feature extraction methods.
- Exploration of dataset characteristics for effective feature selection and dimensionality reduction.
- Application of the pipeline to real-world video datasets in underwater structural health monitoring

Characterization Methodology

The presented methodology is shown in Figure 15, and is motivated by the comprehensive pipeline previously laid out in [88]. Methodological steps include preprocessing of the data, extraction of features, dataset analysis and cleaning, dimensionality reduction, outlier detection and removal, clustering, and ultimately interpretation of the obtained clusters and their correlation with different water types associated with different scenes.

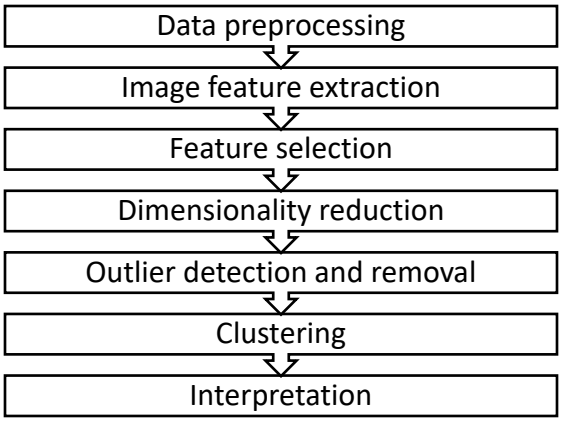

Figure 15. The image characterization pipeline followed in the present study.

Feature extraction

This study considered both local and global low-level features of intrinsic image properties, such as color and texture, as well as complex patterns that emerge from background lighting and scene composition [96]. Extracted attributes are categorized based on their functions and objectives, as shown in Table 3.

Table 3. Overview of image feature extraction techniques employed.

Color and lighting analysis	Texture and clarity analysis	Quality assessment metrics
Color histogram (HSV, yCrCb, Lab)	LBP	UCIQE
Color moments	Variance of Laplacian	CIQI
Background light	Sobel edge detector	

In image analysis, the most salient attributes are often color and lighting features [97,98]. Hence, color profiling is a crucial part of the feature extraction process. Techniques like color histograms [99], color correlograms [100], and color moments [101] are commonly employed to extract color features due to their independence from image size, rotation, and zoom variations [100], and robustness against deformations and scale changes [102].

Texture analysis employs spectral and spatial (statistical) descriptors like Local Binary Patterns (LBP), which evaluates the textural patterns based on the statistical properties of pixel intensities [103,104]. For clarity analysis, accurate blur detection is essential. While deep learning methods such as Convolutional Neural Networks (CNNs) are effective for this purpose, they are also computationally intensive [105]. As an alternative, spatial domain-based methods are utilized due to their lower computational demands [106]. A notable method in this category is the variance of Laplacian, a second-order derivative metric that acts as a high-pass filter [107,108]. This metric can be utilized to evaluate blur by measuring the variance in the image's Laplacian, where higher values indicate sharper images [109]. Additionally, perceptual blurriness metrics involving edge detection are employed [110], notably using the Sobel operator, a first-order derivative method commonly used for its edge-detection capabilities.

Image quality is affected by factors such as the optical performance of the equipment, instrument noise, imaging conditions, and processing techniques [54]. Numerous quality metrics have been presented in the literature, each with its advantages and disadvantages [111,112]. For underwater images, the Underwater Color Image Quality Evaluation (UCIQE) metric [72] is widely used for image quality and color distortion

analysis [61]. In addition to underwater image quality metrics, it is essential to consider metrics designed for non-aquatic mediums. The Color Image Quality Index (CIQI) [73] offers a valuable perspective for evaluating images captured in atmospheric conditions.

Feature selection and dimensionality reduction

A variety of dimensionality reduction techniques (DRTs) are available, each tailored to preserve specific characteristics of the original data, making them appropriate for certain applications while potentially less effective for others [113]. Principal Component Analysis (PCA) is a linear DRT that utilizes eigenvalue decomposition [114]. t-Distributed Stochastic Neighbor Embedding (t-SNE) is a non-linear dimensionality reduction technique that models high-dimensional data by preserving local structures, projecting similar data points close together and dissimilar ones apart in lower-dimensional space [114]. Uniform Manifold Approximation and Projection (UMAP), while similar to t-SNE in goals, employs a different approach by using an exponential probability distribution across any chosen distance function, without normalizing probabilities [114]. UMAP excels in visualization and runtime efficiency compared to t-SNE. Given the distinct behavior of each technique, PCA, t-SNE, and UMAP were each considered for dimensionality reduction.

Feature evaluation and outlier removal

K-means clustering was applied to feature vectors reduced by PCA, t-SNE, and UMAP. The effectiveness of these dimensionality reduction techniques was assessed by examining the clarity and separation of clusters formed, Key metrics used include the Silhouette Score and the Calinski-Harabasz Index and hybrid versions of these metrics found in the literature [115].

Outlier detection and removal is pivotal in data analysis due to the potential of outliers to significantly skew results. In this study, a composite strategy incorporating results from the Modified Z-score, Tukey's method, and Isolation Forest was implemented. This approach identifies outliers by intersecting findings from these methods. One common method is the Modified Z-score, utilizing the median and the median absolute deviation as robust estimators. Tukey's method, also known as the Boxplot technique, calculates outliers based on quartiles rather than the mean and standard deviation. The Isolation Forest technique leverages unlabeled data for outlier detection, isolates observations by randomly selecting a feature and a split value between the maximum and minimum values of that feature. An ensemble of trees is then constructed through recursive partitioning, where the path length to isolate a sample indicates its anomalous nature; shorter paths suggest outliers [116].

Clustering

Three canonical clustering methods are considering in this work: K-means, DBSCAN, and Hierarchical Clustering. K-means is a well-established centroid-based clustering algorithm that partitions the dataset into k distinct, non-overlapping clusters [114,117]. Density-Based Spatial Clustering of Applications with Noise (DBSCAN) excels at identifying clusters of arbitrary shapes and effectively distinguishes outliers. It classifies points as core, border, or noise based on local density [117]. Hierarchical clustering builds a hierarchy of clusters either bottom-up (agglomerative) or top-down (divisive) [114,118].

Experimental Analysis

Datasets

The effectiveness of the proposed pipeline is demonstrated on two distinct datasets. The first one is the Underwater Image Enhancement Benchmark (UIEB) database [119], comprised of 890 underwater images representing a wide range of real-world underwater scenarios including coastal and oceanic environments

with varying visibility and image resolution. The dataset considered in this research consists of 890 underwater images sourced from the Underwater Image Enhancement Benchmark (UIEB) database [119]. These images represented a broad spectrum of real-world underwater scenarios, encompassing both coastal and oceanic environments with varying degrees of visibility and image resolution. The selection of this dataset was driven by its diverse content, which was instrumental in enhancing the generalizability of the developed pipeline. A representative subset of these images is illustrated in Figure 16.

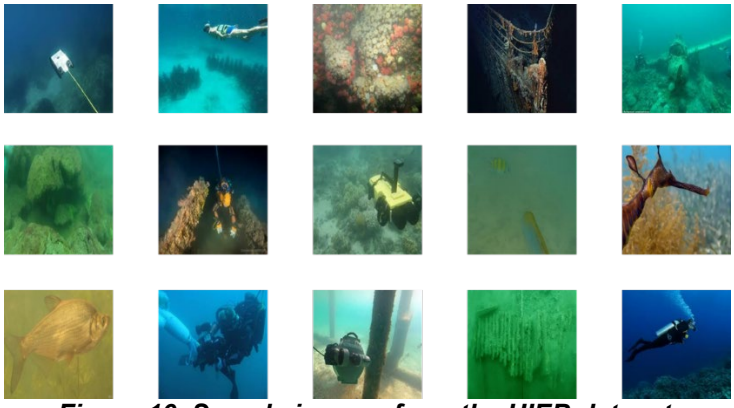

Figure 16. Sample images from the UIEB dataset.

The second dataset is a real-world video dataset captured by the authors during the previously discussed field teating. This dataset was designed to test the pipeline's performance in a maritime infrastructure inspection environment. The primary data collection site was the piers of the bridge. Data capture employed a GoPro Hero 10 action camera mounted on a specialized rig, illustrated in (Figure 9). This rig was equipped with three LED lights and housed in a protective underwater casing to safeguard against impact and damage. Additionally, a Wi-Fi extender was mounted on the backside of the housing to make signal transmission above water possible, allowing for remote control of the camera via the GoPro mobile app. The camera was maneuvered repeatedly between the above and underwater sections of the structure. The data collection spanned three days to vary environmental conditions such as lighting, and tidal and current changes, producing a diverse set of images with varying degrees of water turbidity and lighting quality.

Results on UIEB dataset

To analyze the feature distribution within the dataset, histogram analysis was performed. The histograms demonstrated that the UCIQE quality measure feature effectively differentiated dataset values, whereas some other features could not achieve similar differentiation, as illustrated in Figure 17.

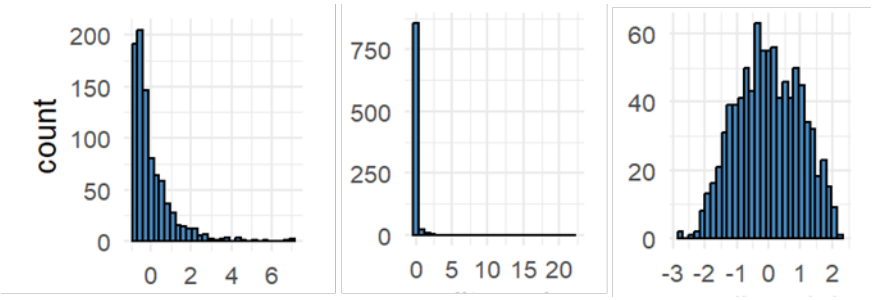

Figure 17. Histogram of scaled dataset for the variance of Laplacian in v channel demonstrating blurriness characteristics (left), the CIQI metrics (middle), and quality UCIQE metrics (right).

The effectiveness of these dimensionality reduction methods was assessed using the Calinski-Harabasz Index and Silhouette Score. As illustrated in Figure 18, PCA demonstrated incremental improvements in Silhouette scores as components increased from 1 to 5, reaching a peak score of 0.14. Further increases in components did not yield additional benefits. The optimal configuration achieved a Silhouette score of 0.13 with 700 neighbors and 3 dimensions. Furthermore, Figure 19 showcases the best hyperparameters for the t-SNE method, encompassing dimensions and perplexity. The peak Silhouette score here reached a lower peak at 0.12 with a perplexity of 90 and 3 dimensions. Consequently, PCA with more than 4 components demonstrated superior performance.

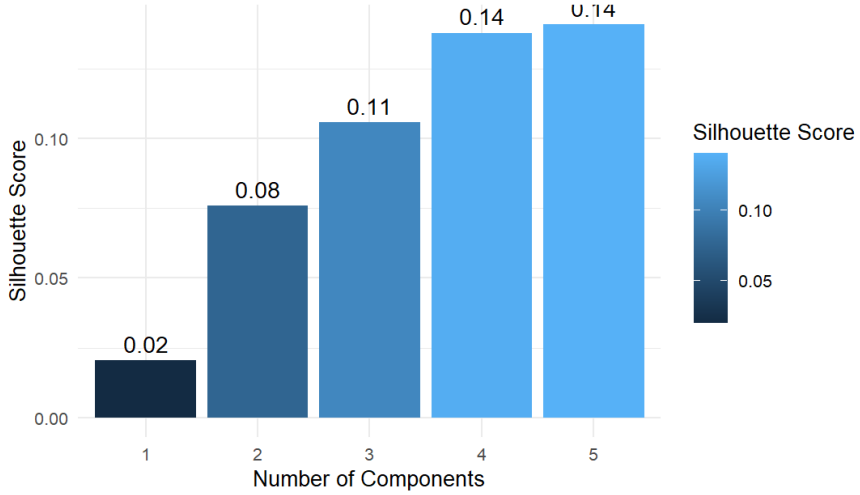

Figure 18. Silhouette scores for different numbers of PCA components.

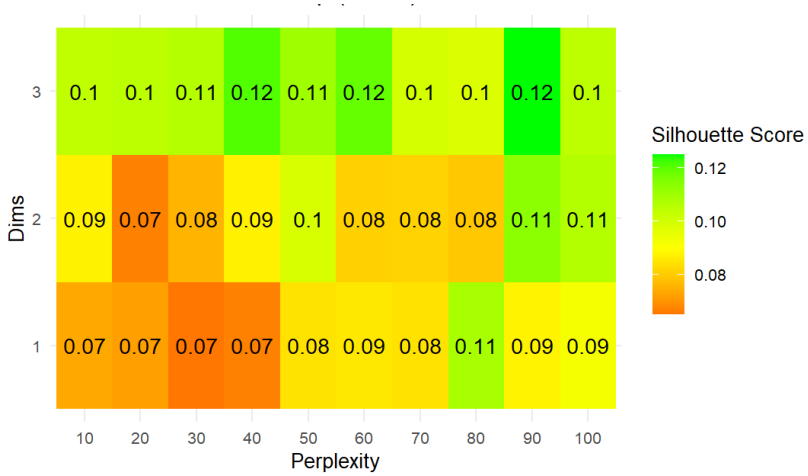

Figure 19. Silhouette score heatmap for different hyperparameters in the t-SNE method.

The excluded outliers detected by each method, resulted in 519, 874, and 822 images remaining for Tukey's method, modified Z-score, and ISF methods, respectively. The highest overlap in outlier identification occurred between the modified Z-score and ISF methods (0.75). The Z-score approach was highly effective at outlier removal, successfully identifying key outliers as demonstrated in Figure 20.

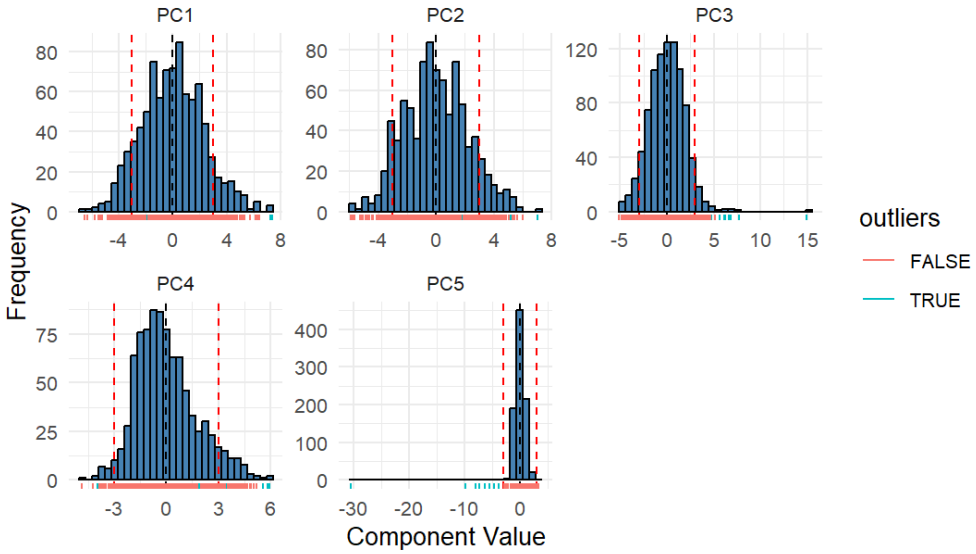

Figure 20. Distribution of detected outliers using the modified Z-score method (Threshold=3).

Following the selection of the remaining part of the dataset after outlier removal, various clustering techniques including K-means, DBSCAN, and Hierarchical Clustering were utilized to determine the best settings. Considering the results obtained through the Silhouette Score, CH Index, and WSS for different clustering algorithms, K-means clustering with five clusters is deemed the most suitable. It is important to highlight that due to the nature of hierarchical clustering, it is more interpretable, which may be advantageous for correlating specific characteristics within the dataset (Figure 21).

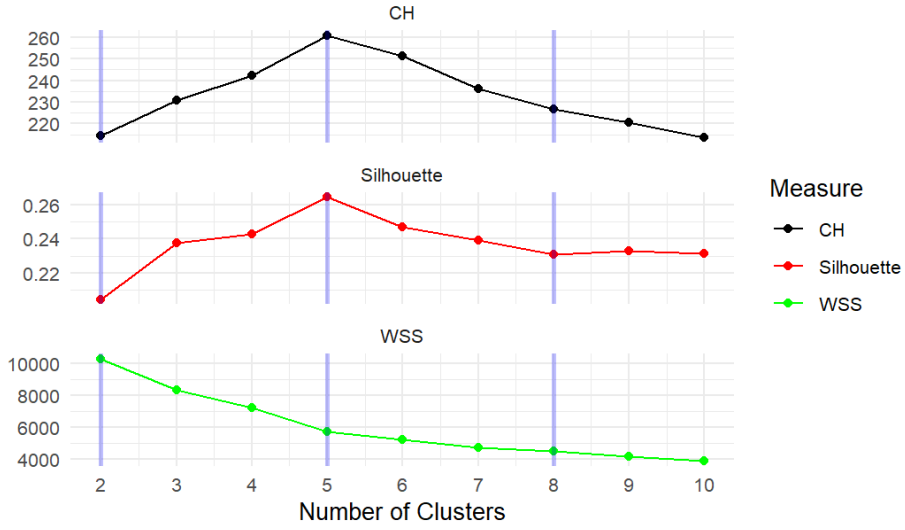

Figure 21. K-means clustering performance evaluation metrics, WSS, CH index, and Silhouette score.

The concluding phase organized images into cluster-specific categories, as depicted in Figure 22. As illustrated, five clusters align with the number of water types in the Jerlov model, and each cluster consists of similar images. While a direct correlation with Jerlov classes could not be established due to the lack of

labeled data, the clustering results offer insights into underwater environmental variations by grouping similar scenes together.

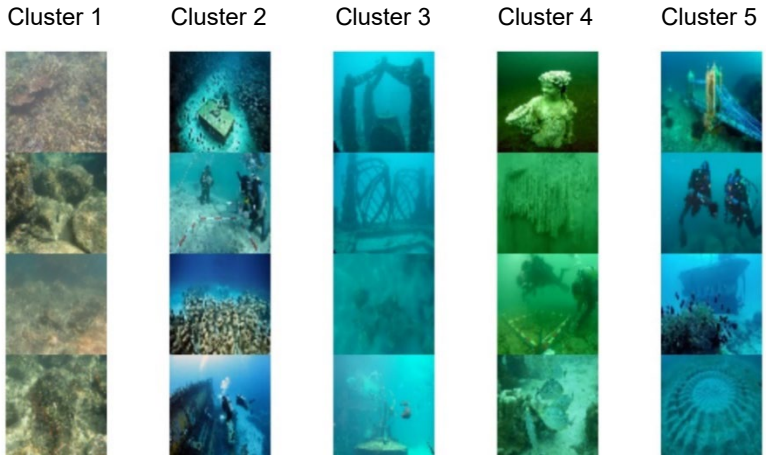

Figure 22. Outcome of the clustering pipeline for the UIEB dataset, with four randomly selected samples from each cluster.

Results from field tests

The images for this dataset were processed through the clustering pipeline as previously applied to the UIEB dataset. The feature analysis, selection, and dimensionality reduction procedures were consistent with those described earlier. Hierarchical Clustering, in particular, showed promising results, as displayed in Figure 23, with optimal clustering revealing three distinct groups. The resultant image clusters are shown in Figure 24, with each row representing a different cluster: images from above water, images devoid of structural content, and images of the piers.

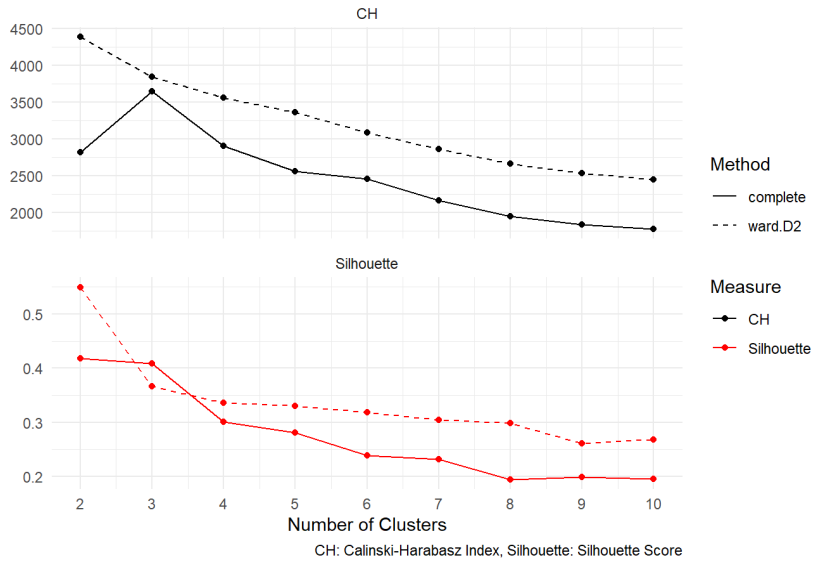

Figure 23. Calinski-Harabasz (CH) scores and silhouette scores for different numbers of clusters in hierarchical clustering for the real-world dataset.

Figure 24. Outcome of the clustering pipeline for the real-world dataset, with randomly selected samples from each cluster.

Conclusions

This study developed and validated a comprehensive clustering pipeline aimed at categorizing underwater images based on their inherent scene characteristics, intending to enhance the interpretability of typically unlabeled underwater imagery. Employing advanced dimensionality reduction techniques and robust clustering algorithms, the methodology systematically analyzed and classified underwater imagery to match water scene types described in the Jerlov model.

The effectiveness of the proposed pipeline was first demonstrated using the well-established Underwater Image Enhancement Benchmark (UIEB) dataset, covering a broad spectrum of underwater conditions. Through meticulous preprocessing, feature extraction, and normalization processes, the pipeline effectively categorized diverse underwater scene characteristics. Dimensionality reduction was achieved using Principal Component Analysis (PCA), t-distributed Stochastic Neighbor Embedding (t-SNE), and Uniform Manifold Approximation and Projection (UMAP), with PCA yielding the most favorable results in terms of cluster coherence and separation as evaluated by the Silhouette Score and Calinski-Harabasz Index.

Additionally, the methodology was applied to a real-world underwater dataset, capturing dynamic scenes above and beneath the water at a water crossing bridge. This practical case study tested the pipeline's applicability to structural health monitoring and condition assessment, showcasing its capability to adapt to varied environmental conditions. The use of K-means and Hierarchical Clustering, in particular, demonstrated the method's adaptability and efficacy across both static images and video data. Looking ahead, future work could involve integrating more sophisticated feature extraction and employing ensemble methods in clustering to further enhance the robustness and accuracy of underwater image categorization.

CHAPTER 4

Integration of digital image correlation and numerical finite element modeling

BRIDGE TEST SPECIFICATIONS

Non-contact measuring systems, including high-resolution (4K) video and laser systems, have become increasingly popular for non-destructive monitoring, particularly for structures like practical steel girder bridges. A video-based method, proposed for fatigue assessment, allows the measurement of displacement responses. The Imetrum Dynamic Monitoring System (DMS), representing vision-based measurement systems, operates as a non-contact tool by capturing videos and recording measurement data through relative motion points on the video file. DMS employs two-dimensional Digital Image Correlation (2D DIC) and consists of cameras and a processor. This technology is advantageous in scenarios where traditional sensors are impractical, enabling measurements in challenging cases. Its non-intrusive nature is especially valuable for applications where minimizing impact on the structure is crucial, such as historic structures or delicate materials.

The use of vision-based measurements, notably in bridge load testing, eliminates the need for extensive sensor installations. Digital imaging, capable of capturing data from multiple points of interest, has become crucial for evaluating in-situ conditions in aging bridges in the United States. While the evolving technological landscape provides enhanced data capture tools and repeatable post-processing using video-based images, it is important to note limitations in vision-based measurement deployment, including considerations for lighting conditions, skew effect, and field of view when using DIC techniques for point-to-point tracking of displacements.

The structural evaluation of a bridge in Virginia, located around the DC area, is the focus of this study as a case study undertaken in collaboration with a team at George Mason University (GMU). In Figure 25, an aerial view of the bridge with highlighting the camera locations is depicted. This collaborative project involves the deployment of the Imetrum DMS system to monitor the bridge and utilize the recorded data for creating and calibrating a digital twin model of the current structure.

Figure 25. Aerial Google view of the bridge and the location of the deployments of the DMS

Several challenges arise during the data recording process. These include variations in lighting due to partly cloudy weather, leading to false motions detected by the camera. Additionally, physical obstacles like seagulls flying within the camera's field of view can cause the DMS to lose track of points at intermittent intervals. The distance from the bridge imposes limitations on calibration, relying solely on known distances such as span and pier lengths. Figure 26 demonstrates the span lengths in a view from the harbor deck. Vibrations from the waves affect the deck where cameras are mounted on tripods, adding complexity to capturing deformations. Furthermore, the need for targetless tracking points poses a unique challenge for measurement.

Creating a finite element (FE) model of the bridge presented its own set of challenges, particularly concerning unknown loading conditions associated with the weight, location, and speed of passing vehicles. The goal is to develop the FE model as accurately as possible, relying on the plans provided.

Figure 26. The bridge and the monitored spans with their length from the harbor deck's view

Trucks typically carry a higher weight, leading to increased loads on the bridge and, consequently, higher deflection. This facilitates the DMS in capturing deflection during tests. In Figure 27, the passage of an 18-wheel truck over the bridge is captured within the field of view of the cameras. Two passes of the trucks are utilized as a load source for the reference point during model calibration. The calibration primarily involves adjusting the boundary conditions, restraints, and joints.

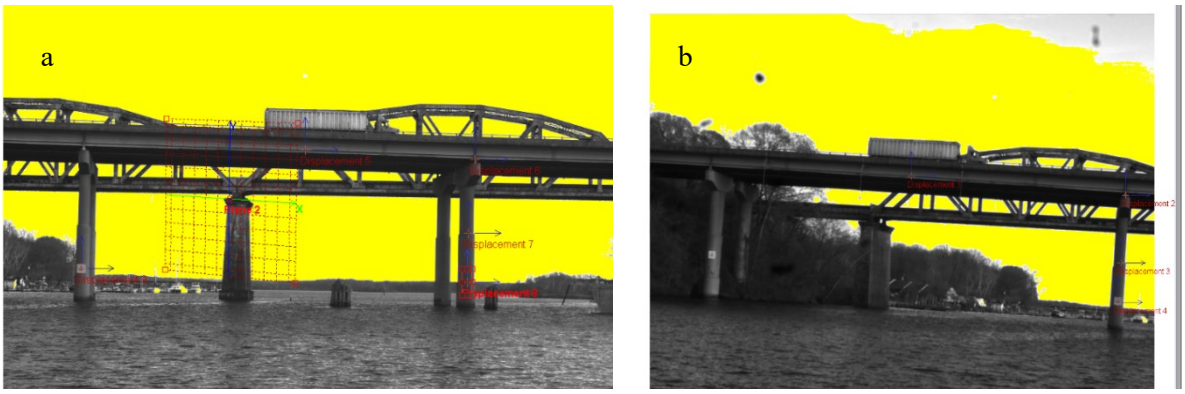

Figure 27. Imetrum DMS field of view for (a) camera 1 looking towards the third span and (b) camera 2 looking towards the second span.

The FE model was constructed using CSI Bridge software, with dimensions adjusted based on the provided drawing plans. Trucks were assumed to carry 70% of their allowed maximum capacity while moving at the maximum allowable speed of 35 mph on the bridge.

Verification of the Vision-Based Measurement System

Before conducting the field test, we implemented verification tests to evaluate the effectiveness of the vision-based measuring system (DIC) and validate measurement accuracy. These tests were performed on a bi-directional shake table at the ATLSS Engineering Research Center at Lehigh University. The specialized test involved applying harmonic motions and utilizing known ground motion displacements derived from widely recognized ground motion data. The specific test conditions and parameters are outlined below:

Table 4. Lehigh Shake table tests description.

Test Number	Description	Test Type
1	Circle + Rotation EW and NS 4in (101.6mm), 5 degree, 0.5Hz	2D (increasing amplitude)
2	Manjil Iran	Ground Motion

The capability of the DIC system in capturing the precise data was assessed by thoroughly comparing true data (i.e., displacement values) with the measurements. The test setup configurations and camera field of view are shown in Figure 28 where the camera was mounted on the catwalk above the shake table with no perspective and a capturing data frequency set at 100 Hz.

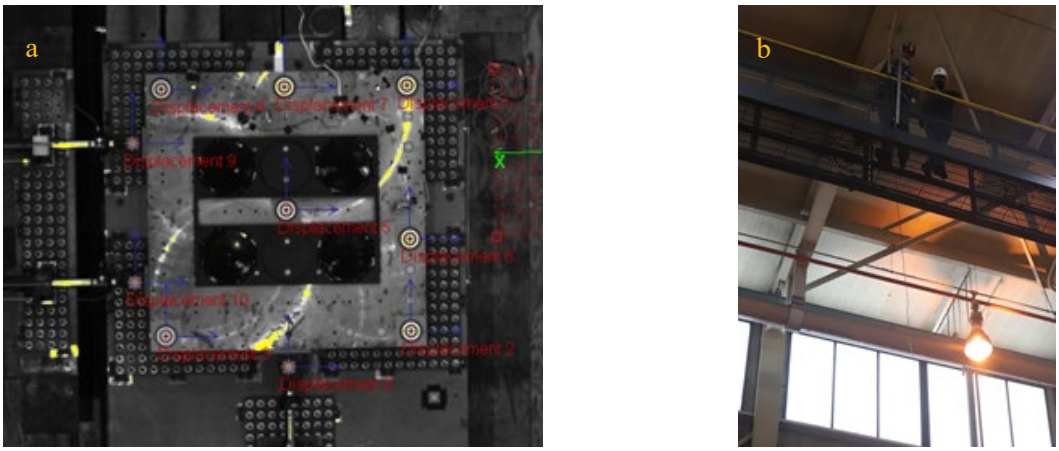

Figure 28. The shake table test configuration, (a) DMS field of view (b) camera located on the catwalk above the table.

The DIC system, Imetrum DMS, demonstrated satisfactory performance in capturing the motion of the shake table under both harmonic and ground motion scenarios. Figure 29 visually presents the Imetrum displacement in conjunction with the true displacement data from the shake table in the time domain. This depiction underscores the system's capability to precisely record dynamic movements, affirming its effectiveness in accurately representing the observed motions.

The results obtained from these tests also demonstrate agreement in the frequency domain. Figure 30 illustrates a comparison between the captured data results from the shake table tests and the true displacements in the frequency domain. The displacement captured in the Y-axis during Test 1 highlights the DMS's capability to accurately capture frequencies. Test 1 results affirm the DMS's ability to track motion in two dimensions simultaneously. Test 2, which involves earthquake ground motion monitoring, further confirms the DMS's capability to monitor ground motions across a range of frequencies.

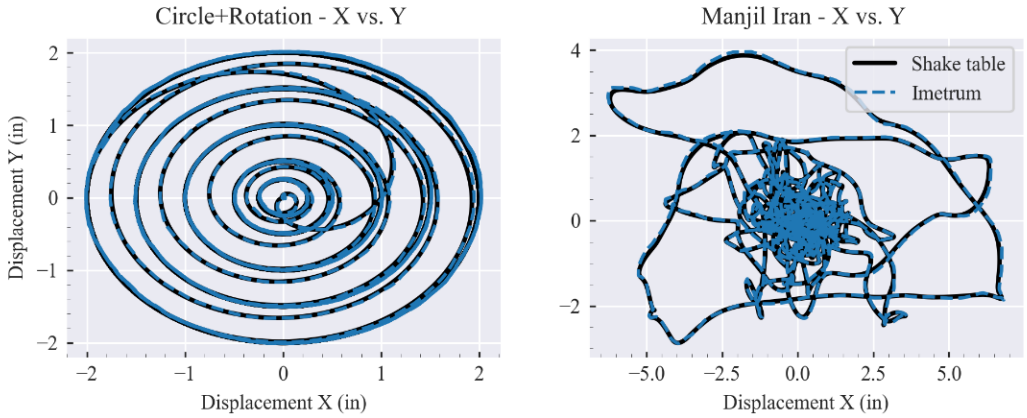

Figure 29. Displacement (1in.=25.4mm) captured in the time domain with the DIC in the shake table tests. (left) and (right) in X direction versus Y for tests 1 and 2 in Table 4.

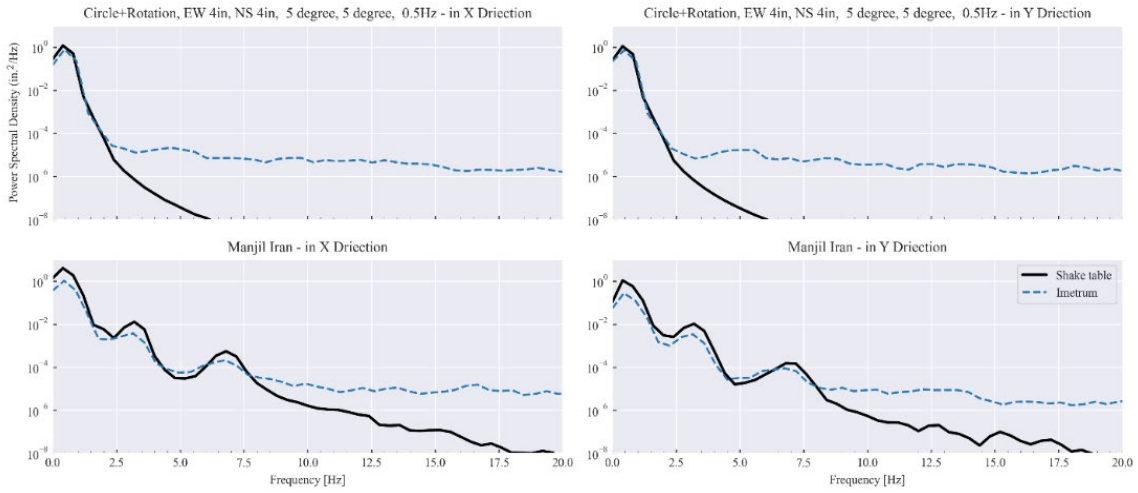

Figure 30. Frequency domain of captured displacement with the DIC in the shake table tests in X-axis (left) and Y-axis (right) (1in.=25.4mm)

RESULTS

After verifying the accuracy of the DMS in capturing the displacement in time and frequency domain, this section presents the results obtained from the field measurement and model updating using those field measurements which were applied to the bridge case study. The maximum deflection on the midspans was monitored and used as the target for matching the model results with field measurements. The Finite Element (FE) model was constructed according to the plan, with the maximum truck load assumed to be 70% of the standard.

In Figure 31 (top), the midspan deflection for the second and third spans of the bridge is shown for two different truck passes, compared to the FE model results. The results exhibit promising agreements, suggesting that this method can be effectively utilized for updating models and creating a digital twin of the structure.

From monitoring of the bridge pier, the results from the Finite Element (FE) model, depicted in Figure 31 bottom right, shows the deflection of the top of the second pier in the bridge. It indicates that the anticipated displacement values for that point in all directions are below 0.02 inches. Conversely, the field measurements, Figure 31 bottom left, present similar outcomes during truck passes for the vertical displacement of the top of the pier. Due to the limited deflection range and field constraints, such as the considerable distance, DMS was unable to record the deflection for that specific point.

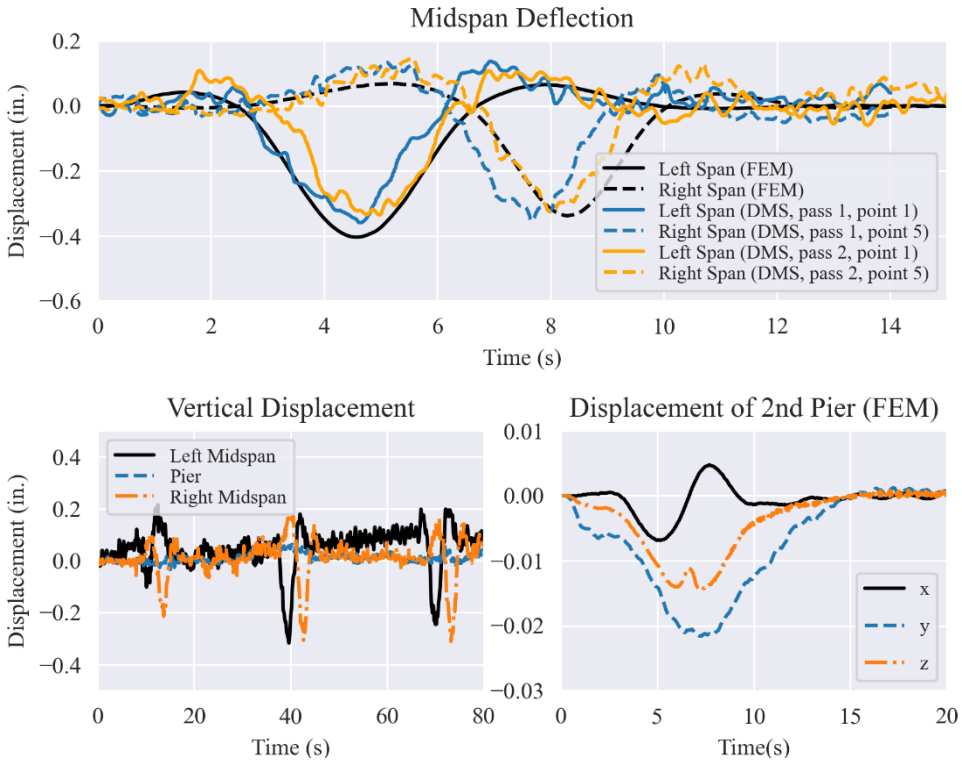

Figure 31. Comparative analysis of bridge deflection: (top) midspan deflection in FE model and field measurements, (bottom right) FE model results (bottom left) field measurements of the second pier in the bridge (1in.=25.4mm)

CHAPTER 5

Recommendations

CONCLUSION

In this study, the transformative potential of video-based image measurements, particularly employing Digital Image Correlation (DIC), in the realm of structural health monitoring for bridges was explored. The integration of video-based measurements with structural models and the subsequent creation of digital twins offers a groundbreaking methodology for accurate and dynamic representation of structural behavior. The verification tests conducted on a bi-directional shake table with harmonic motions and utilizing known ground motion displacements demonstrated the effectiveness and accuracy of the vision-based measuring system (DIC).

This study focused on a multi-span steel girder bridge, revealing promising results in monitoring midspan deflections and bridge pier behavior during truck passes. The use of the DMS proved the advantages of vision-based measurements, particularly in scenarios where traditional sensors may be impractical or intrusive. The outcomes of this research emphasize the potential of video-based measurements in updating structural models, creating digital twins, and enhancing decision-making processes in bridge asset management. By providing insights into existing conditions, facilitating model calibration, and offering a non-intrusive and cost-effective approach, this innovative methodology holds significant promise for the future of structural engineering and infrastructure management. As technology continues to evolve, integrating vision-based measurement systems into standard practices could revolutionize the way we monitor, assess, and ensure the longevity and safety of critical infrastructure.

References

1. FHWA (Federal Highway Administration) (2004) National bridge inspection standards. *Federal Register*, **69** (239), 74419–39.
2. Oregon Department of Transportation (2020) Inspection trucks help us look under the bridge.
3. Command, U.S.I.-P. (2017) U.S. Navy divers conduct underwater pier survey in Apra Harbor, Guam.
4. Han, J., Park, J., and Kim, J. (2014) Three-dimensional reconstruction of bridge structures above the waterline with an unmanned surface vehicle. *2014 IEEE/RSJ International Conference on Intelligent Robots and Systems*, 2273–2278.
5. Lattanzi, D., and Miller, G.R. (2015) 3D Scene Reconstruction for Robotic Bridge Inspection. *Journal of Infrastructure Systems*, **21** (2), 04014041.
6. Mitchell, T., Miller, C., and Lee, T. (2011) Multibeam surveys extended above the waterline. *Proceedings of WEDA Technical Conference and Texas A&M Dredging Seminar*.
7. Sutter, B., Lelevé, A., Pham, M.T., Gouin, O., Jupille, N., Kuhn, M., Lulé, P., Michaud, P., and Rémy, P. (2018) A semi-autonomous mobile robot for bridge inspection. *Automation in Construction*, **91**, 111–119.
8. Lagudi, A., Bianco, G., Muzzupappa, M., and Bruno, F. (2016) An alignment method for the integration of underwater 3D data captured by a stereovision system and an acoustic camera. *Sensors*, **16** (4), 536.
9. Vasilijevic, A., Kapetanović, N., and Mišković, N. (2020) Inspection of Submerged Structures. *Global Trends in Testing, Diagnostics & Inspection for 2030*.
10. Wang, J., Bai, S., and Englot, B. (2017) Underwater localization and 3D mapping of submerged structures with a single-beam scanning sonar. *2017 IEEE International Conference on Robotics and Automation (ICRA)*, 4898–4905.
11. Chen, B., Yang, Y., Zhou, J., Zhuang, Y., and McFarland, M. (2021) Damage detection of underwater foundation of a Chinese ancient stone arch bridge via sonar-based techniques. *Measurement*, **169**, 108283.
12. Mattei, G., Troisi, S., Aucelli, P.P., Pappone, G., Peluso, F., and Stefanile, M. (2018) Sensing the submerged landscape of Nisida Roman Harbour in the Gulf of Naples from integrated measurements on a USV. *Water*, **10** (11), 1686.
13. Han, J., Kang, M., Wang, J., and Kim, J. (2016) Three-dimensional reconstruction of a semi-submersible offshore platform with an unmanned surface vehicle. *OCEANS 2016-Shanghai*, 1–6.
14. Han, J., and Kim, J. (2018) Three-dimensional reconstruction of a marine floating structure with an unmanned surface vessel. *IEEE Journal of Oceanic Engineering*, **44** (4), 984–996.
15. Moisan, E., Heinkelé, C., Foucher, P., Charbonnier, P., Grussenmeyer, P., Guillemin, S., and Koehl, M. (2021) Combining photogrammetric and bathymetric data to build a 3D model of a canal tunnel. *The Photogrammetric Record*, **36** (175), 202–223.
16. Moisan, E., Charbonnier, P., Foucher, P., Grussenmeyer, P., Guillemin, S., and Koehl, M. (2015) Adjustment of sonar and laser acquisition data for building the 3D reference model of a canal tunnel. *Sensors*, **15** (12), 31180–31204.
17. Murphy, R.R., Steimle, E., Griffin, C., Cullins, C., Hall, M., and Pratt, K. (2008) Cooperative use of unmanned sea surface and micro aerial vehicles at Hurricane Wilma. *Journal of Field Robotics*, **25** (3), 164–180.
18. Murphy, R.R., Dreger, K.L., Newsome, S., Rodocker, J., Slaughter, B., Smith, R., Steimle, E., Kimura, T., Makabe, K., Kon, K., and others (2012) Marine heterogeneous multirobot systems at the great Eastern Japan Tsunami recovery. *Journal of Field Robotics*, **29** (5), 819–831.

19. Hosamo, H.H., and Hosamo, M.H. (2022) Digital Twin Technology for Bridge Maintenance using 3D Laser Scanning: A Review. *Advances in Civil Engineering*, **2022** (1), 2194949.
20. Marks, R., Gillam, C., Clarke, A., Armstrong, J., and Pullin, R. (2017) Damage detection in a composite wind turbine blade using 3D scanning laser vibrometry. *Proceedings of the Institution of Mechanical Engineers, Part C: Journal of Mechanical Engineering Science*, **231** (16), 3024–3041.
21. Baqersad, J., Poozesh, P., Niezrecki, C., and Avitabile, P. (2017) Photogrammetry and optical methods in structural dynamics – A review. *Mechanical Systems and Signal Processing*, **86**, 17–34.
22. Ngeljaratan, L., and Moustafa, M.A. (2020) Implementation and Evaluation of Vision-Based Sensor Image Compression for Close-Range Photogrammetry and Structural Health Monitoring. *Sensors*, **20** (23).
23. Zhao, S., Kang, F., Li, J., and Ma, C. (2021) Structural health monitoring and inspection of dams based on UAV photogrammetry with image 3D reconstruction. *Automation in Construction*, **130**, 103832.
24. Lee, J., Lee, K.-C., Lee, S., Lee, Y.-J., and Sim, S.-H. (2019) Long-term displacement measurement of bridges using a LiDAR system. *Structural Control and Health Monitoring*, **26** (10), e2428.
25. Oats, R.C., Dai, Q., and Head, M. (2022) Digital Image Correlation Advances in Structural Evaluation Applications: A Review. *Pract. Period. Struct. Des. Constr.*, **27** (4), 03122007.
26. Thai, H.-T. (2022) Machine learning for structural engineering: A state-of-the-art review. *Structures*, **38**, 448–491.
27. Ye, X.W., Dong, C.Z., and Liu, T. (2016) A Review of Machine Vision-Based Structural Health Monitoring: Methodologies and Applications. *Journal of Sensors*, **2016**, e7103039.
28. DuBose, T., Safari, S., Shenton, H.W., Tatar, J., Chajes, M.J., Karam, J., Hastings, J.N., and Head*, M.H. (2022) Diagnostic load testing and assessment of a rehabilitated culvert with spray applied pipe liner, in *Bridge Safety, Maintenance, Management, Life-Cycle, Resilience and Sustainability*, CRC Press.
29. Safari, S., Head, M.H., and DuBose, T. (2023) Vision-Based Measurements for Monitoring a Rehabilitated Corrugated Metal Pipe Culvert. *Structures Congress 2023*, 416–434.
30. Head, M., Safari, S., Aloqaily, W., and Obayes, S. (2023) Non-contact structural monitoring of a railway bridge, in *Risk-Based Strategies for Bridge Maintenance*, CRC Press.
31. Monique H. Head, L.T. (2022) Live Load Distribution of Slab-on-Girder Bridges Using Vision-based Measurements. *ACI Symposium Publication*, **352**.
32. Janeliukstis, R., and Chen, X. (2021) Review of digital image correlation application to large-scale composite structure testing. *Composite Structures*, **271**, 114143.
33. Chen, J.G., Wadhwa, N., Cha, Y.-J., Durand, F., Freeman, W.T., and Buyukozturk, O. (2015) Modal identification of simple structures with high-speed video using motion magnification. *Journal of Sound and Vibration*, **345**, 58–71.
34. Reagan, D., Sabato, A., and Niezrecki, C. (2018) Feasibility of using digital image correlation for unmanned aerial vehicle structural health monitoring of bridges. *Structural Health Monitoring*, **17** (5), 1056–1072.
35. Jiang, S., Wang, Y., Zhang, J., and Zheng, J. (2023) Full-field deformation measurement of structural nodes based on panoramic camera and deep learning-based tracking method. *Computers in Industry*, **146**, 103840.
36. Ridao, P., Carreras, M., Ribas, D., and Garcia, R. (2010) Visual inspection of hydroelectric dams using an autonomous underwater vehicle. *Journal of Field Robotics*, **27** (6), 759–778.
37. Liu, Y., Hajj, M., and Bao, Y. (2022) Review of robot-based damage assessment for offshore wind turbines. *Renewable and Sustainable Energy Reviews*, **158**, 112187.
38. Sutter, B., Lelevé, A., Pham, M.T., Gouin, O., Jupille, N., Kuhn, M., Lulé, P., Michaud, P., and Rémy, P. (2018) A semi-autonomous mobile robot for bridge inspection. *Automation in Construction*, **91**, 111–119.
39. DeVault, J.E. (2000) Robotic system for underwater inspection of bridge piers. *IEEE Instrum. Meas. Mag.*, **3** (3), 32–37.

40. Halder, S., and Afsari, K. (2023) Robots in Inspection and Monitoring of Buildings and Infrastructure: A Systematic Review. *Applied Sciences*, **13** (4).
41. Jo, B.-W., Lee, Y.-S., Kim, J.-H., and Yoon, K.-W. (2018) A Review of Advanced Bridge Inspection Technologies Based on Robotic Systems and Image Processing. *International Journal of Contents*, **14** (3), 17–26.
42. Falorca, J.F., and Lanzinha, J.C.G. (2020) Facade inspections with drones–theoretical analysis and exploratory tests. *IJBPA*, **39** (2), 235–258.
43. La, H.M., Gucunski, N., Kee, S.-H., and Nguyen, L.V. (2015) Data analysis and visualization for the bridge deck inspection and evaluation robotic system. *Visualization in Engineering*, **3** (1), 6.
44. Prasanna, P., Dana, K.J., Gucunski, N., Basily, B.B., La, H.M., Lim, R.S., and Parvardeh, H. (2016) Automated Crack Detection on Concrete Bridges. *IEEE Transactions on Automation Science and Engineering*, **13** (2), 591–599.
45. Seto, M.L. (ed.) (2013) *Marine Robot Autonomy*, Springer New York, New York, NY.
46. Xanthidis, M., Joshi, B., O'Kane, J.M., and Rekleitis, I. (2022) Multi-Robot Exploration of Underwater Structures. *IFAC-PapersOnLine*, **55** (31), 395–400.
47. J. Choi, Y. Lee, T. Kim, J. Jung, and H. -T. Choi (2017) Development of a ROV for visual inspection of harbor structures. *2017 IEEE Underwater Technology (UT)*, 1–4.
48. Giordano, F., Mattei, G., Parente, C., Peluso, F., and Santamaria, R. (2016) Integrating Sensors into a Marine Drone for Bathymetric 3D Surveys in Shallow Waters. *Sensors*, **16** (1).
49. Sankpal, S., and Deshpande, S. (2016) A review on image enhancement and color correction techniques for underwater images. *Advances in Computer Science and Technology*, **9**, 11–23.
50. O'Byrne, M., Schoefs, F., Pakrashi, V., and Ghosh, B. (2018) An underwater lighting and turbidity image repository for analysing the performance of image-based non-destructive techniques. *Structure and Infrastructure Engineering*, **14** (1), 104–123.
51. Duarte, A., Codevilla, F., Gaya, J.D.O., and Botelho, S.S.C. (2016) A dataset to evaluate underwater image restoration methods. *OCEANS 2016 - Shanghai*, 1–6.
52. Peng, Y.-T., and Cosman, P.C. (2017) Underwater Image Restoration Based on Image Blurriness and Light Absorption. *IEEE Transactions on Image Processing*, **26** (4), 1579–1594.
53. Swirski, Y., and Schechner, Y.Y. (2013) 3Deflicker from motion. *IEEE International Conference on Computational Photography (ICCP)*, 1–9.
54. Wang, Y., Song, W., Fortino, G., Qi, L.-Z., Zhang, W., and Liotta, A. (2019) An Experimental-Based Review of Image Enhancement and Image Restoration Methods for Underwater Imaging. *IEEE Access*, **7**, 140233–140251.
55. Bianco, G., Gallo, A., Bruno, F., and Muzzupappa, M. (2013) A Comparative Analysis between Active and Passive Techniques for Underwater 3D Reconstruction of Close-Range Objects. *Sensors*, **13** (8), 11007–11031.
56. Monterroso Muñoz, A., Moron-Fernández, M.-J., Cascado-Caballero, D., Diaz-del-Rio, F., and Real, P. (2023) Autonomous Underwater Vehicles: Identifying Critical Issues and Future Perspectives in Image Acquisition. *Sensors*, **23** (10), 4986.
57. Li, C.Y., Mazzon, R., and Cavallaro, A. (2020) Underwater image filtering: methods, datasets and evaluation.
58. Padmavathi, D.G., Subashini, D.P., Kumar, M.M.M., and Thakur, S.K. (2010) Comparison of Filters used for Underwater Image Pre-Processing.
59. Henke, B., Vahl, M., and Zhou, Z. (2013) Removing color cast of underwater images through non-constant color constancy hypothesis. *2013 8th International Symposium on Image and Signal Processing and Analysis (ISPA)*, 20–24.
60. Ancuti, C.O., Ancuti, C., De Vleeschouwer, C., and Bekaert, P. (2018) Color Balance and Fusion for Underwater Image Enhancement. *IEEE Trans. on Image Process.*, **27** (1), 379–393.
61. Yang, M., Hu, J., Li, C., Rohde, G., Du, Y., and Hu, K. (2019) An In-Depth Survey of Underwater Image Enhancement and Restoration. *IEEE Access*, **7**, 123638–123657.

62. Kim, H.-G., Seo, J., and Kim, S.M. (2022) Underwater Optical-Sonar Image Fusion Systems. *Sensors*, **22** (21), 8445.
63. Bingham, B., Foley, B., Singh, H., Camilli, R., Delaporta, K., Eustice, R., Mallios, A., Mindell, D., Roman, C., and Sakellariou, D. (2010) Robotic tools for deep water archaeology: Surveying an ancient shipwreck with an autonomous underwater vehicle. *Journal of Field Robotics*, **27** (6), 702–717.
64. Lagudi, A., Bianco, G., Muzzupappa, M., and Bruno, F. (2016) An Alignment Method for the Integration of Underwater 3D Data Captured by a Stereovision System and an Acoustic Camera. *Sensors*, **16** (4), 536.
65. Li, C., Quo, J., Pang, Y., Chen, S., and Wang, J. (2016) Single underwater image restoration by blue-green channels dehazing and red channel correction. *2016 IEEE International Conference on Acoustics, Speech and Signal Processing (ICASSP)*, 1731–1735.
66. Berman, D. Diving into Haze-Lines: Color Restoration of Underwater Images. 12.
67. Ye, X., Li, Z., Sun, B., Wang, Z., Xu, R., Li, H., and Fan, X. (2020) Deep Joint Depth Estimation and Color Correction From Monocular Underwater Images Based on Unsupervised Adaptation Networks. *IEEE Trans. Circuits Syst. Video Technol.*, **30** (11), 3995–4008.
68. Zhao, X., Jin, T., and Qu, S. (2015) Deriving inherent optical properties from background color and underwater image enhancement. *Ocean Engineering*, **94**, 163–172.
69. Silva Vaz, E., de Toledo, E.F., and Drews, P.L.J. (2020) Underwater Depth Estimation based on Water Classification using Monocular Image. *2020 Latin American Robotics Symposium (LARS), 2020 Brazilian Symposium on Robotics (SBR) and 2020 Workshop on Robotics in Education (WRE)*, 1–6.
70. O'Byrne, M., Ghosh, B., Schoefs, F., and Pakrashi, V. (2020) Applications of Virtual Data in Subsea Inspections. *JMSE*, **8** (5), 328.
71. Yedida, R., Yang, X., and Menzies, T. (2022) Old but Gold: Reconsidering the value of feedforward learners for software analytics.
72. Yang, M., and Sowmya, A. (2015) An Underwater Color Image Quality Evaluation Metric. *IEEE Transactions on Image Processing*, **24** (12), 6062–6071.
73. Fu, Y.-Y. (2006) Color image quality measures and retrieval.
74. Panetta, K., Gao, C., and Agaian, S. (2013) No reference color image contrast and quality measures. *IEEE Transactions on Consumer Electronics*, **59** (3), 643–651.
75. Raihan A, J., Abas, P.E., and De Silva, L.C. (2021) A Simulated Water Type Dataset (SWTD) Based on Jerlov Water Types for Underwater Image Quality Analysis. *Journal of Advances in Information Technology*, **12** (4), 334–341.
76. Diamanti, E., and Ødegård, Ø. (2024) Visual sensing on marine robotics for the 3D documentation of Underwater Cultural Heritage: A review. *Journal of Archaeological Science*, **166**, 105985.
77. Xu, Y., and Stilla, U. (2021) Toward Building and Civil Infrastructure Reconstruction From Point Clouds: A Review on Data and Key Techniques. *IEEE J. Sel. Top. Appl. Earth Observations Remote Sensing*, **14**, 2857–2885.
78. Hu, K., Wang, T., Shen, C., Weng, C., Zhou, F., Xia, M., and Weng, L. (2023) Overview of Underwater 3D Reconstruction Technology Based on Optical Images. *JMSE*, **11** (5), 949.
79. Mitchell, T.J., Miller, C.A., and Lee, T.P. (2011) Multibeam Surveys Extended Above the Waterline. 9.
80. Moisan, E., Charbonnier, P., Foucher, P., Grussenmeyer, P., Guillemin, S., and Koehl, M. (2015) Adjustment of Sonar and Laser Acquisition Data for Building the 3D Reference Model of a Canal Tunnel. *Sensors*, **15** (12), 31180–31204.
81. Hake, F., Göttert, L., Neumann, I., and Alkhatib, H. (2022) Using Machine-Learning for the Damage Detection of Harbour Structures. *Remote Sensing*, **14** (11), 2518.
82. Menna, F., Nocerino, E., and Remondino, F. (2018) Photogrammetric Modelling of Submerged Structures: Influence of Underwater Environment and Lens Ports on Three-Dimensional (3D) Measurements, in *Latest Developments in Reality-Based 3D Surveying and Modelling*, MDPI.

83. Nocerino, E., and Menna, F. (2020) Photogrammetry: Linking the World across the Water Surface. *JMSE*, **8** (2), 128.
84. Chu, T., Ranson, W., and Sutton, M. (1985) Applications of digital-image-correlation techniques to experimental mechanics. *Experimental Mechanics*, **25**, 232–244.
85. Nonis, C., Niezrecki, C., Yu, T.-Y., Ahmed, S., Su, C.-F., and Schmidt, T. (2013) Structural health monitoring of bridges using digital image correlation. 869507.
86. Sutton, M., Wolters, W., Peters, W., Ranson, W., and McNeill, S. (1983) Determination of displacements using an improved digital correlation method. *Image and Vision Computing*, **1** (3), 133–139.
87. Imetrum. *Imetrum*.
88. Sun Limin, Shang Zhiqiang, Xia Ye, Bhowmick Sutanu, and Nagarajaiah Satish (2020) Review of Bridge Structural Health Monitoring Aided by Big Data and Artificial Intelligence: From Condition Assessment to Damage Detection. *Journal of Structural Engineering*, **146** (5), 04020073.
89. Chen, Y., Li, Q., Gong, S., Liu, J., and Guan, W. (2022) UV3D: Underwater Video Stream 3D Reconstruction Based on Efficient Global SFM. *Applied Sciences*, **12** (12), 5918.
90. Asha Paul, M.K., Kavitha, J., and Jansi Rani, P.A. (2018) Key-Frame Extraction Techniques: A Review. *CSENG*, **11** (1), 3–16.
91. Li, J., Skinner, K.A., Eustice, R.M., and Johnson-Roberson, M. (2017) WaterGAN: Unsupervised Generative Network to Enable Real-time Color Correction of Monocular Underwater Images. *IEEE Robot. Autom. Lett.*, 1–1.
92. Graves, W., Aminfar, K., and Lattanzi, D. (2022) Full-Scale Highway Bridge Deformation Tracking via Photogrammetry and Remote Sensing. *Remote Sensing*, **14** (12), 2767.
93. Graves, W., Nahshon, K., Aminfar, K., and Lattanzi, D. (2023) Finite element model updating with quantified uncertainties using point cloud data. *DCE*, **4**, e16.
94. Shortis, M. (2015) Calibration Techniques for Accurate Measurements by Underwater Camera Systems. *Sensors*, **15** (12), 30810–30826.
95. Guo, T., Capra, A., Troyer, M., Gruen, A., Brooks, A.J., Hench, J.L., Schmitt, R.J., Holbrook, S.J., and Dubbini, M. (2016) Accuracy Assessment of Underwater Photogrammetric Three Dimensional Modelling for Coral Reefs. *The International Archives of the Photogrammetry, Remote Sensing and Spatial Information Sciences*, **XLI-B5**, 821–828.
96. Taheri, F., Rahbar, K., and Salimi, P. (2023) Effective features in content-based image retrieval from a combination of low-level features and deep Boltzmann machine. *Multimed Tools Appl*, **82** (24), 37959–37982.
97. Pradhan, J., Kumar, S., Pal, A.K., and Banka, H. (2020) Texture and colour region separation based image retrieval using probability annular histogram and weighted similarity matching scheme. *IET Image Processing*, **14** (7), 1303–1315.
98. Ping Tian, D. (2013) A review on image feature extraction and representation techniques. *International Journal of Multimedia and Ubiquitous Engineering*, **8** (4), 385–396.
99. Jain, A.K., and Vailaya, A. (1996) Image retrieval using color and shape. *Pattern Recognition*, **29** (8), 1233–1244.
100. Jing Huang, Kumar, S.R., Mitra, M., Wei-Jing Zhu, and Zabih, R. (1997) Image indexing using color correlograms. *Proceedings of IEEE Computer Society Conference on Computer Vision and Pattern Recognition*, 762–768.
101. Mufarroha, F.A., Anamisa, D.R., and Hapsani, A.G. (2020) Content Based Image Retrieval Using Two Color Feature Extraction. *J. Phys.: Conf. Ser.*, **1569** (3), 032072.
102. Tian, Y., Fang, M., and Kaneko, S. (2022) Absent Color Indexing: Histogram-Based Identification Using Major and Minor Colors. *Mathematics*, **10** (13), 2196.
103. Tekli, J. (2022) An overview of cluster-based image search result organization: background, techniques, and ongoing challenges. *Knowl Inf Syst*, **64** (3), 589–642.

104. Singh, A., Sunkaria, R.K., and Kaur, A. (2022) A Review on Local Binary Pattern Variants. *Proceedings of First International Conference on Computational Electronics for Wireless Communications*, 545–552.
105. Khan, A., Javed, A., Irtaza, A., and Mahmood, M.T. (2021) A Robust Approach for Blur and Sharp Regions' Detection Using Multisequential Deviated Patterns. *International Journal of Optics*, **2021**, e2785225.
106. Zhu, M., Yu, L., Wang, Z., Ke, Z., and Zhi, C. (2023) Review: A Survey on Objective Evaluation of Image Sharpness. *Applied Sciences*, **13** (4), 2652.
107. Bansal, R., Raj, G., and Choudhury, T. (2016) Blur image detection using Laplacian operator and Open-CV. *2016 International Conference System Modeling & Advancement in Research Trends (SMART)*, 63–67.
108. Tai, S.-C., and Yang, S.-M. (2008) A fast method for image noise estimation using Laplacian operator and adaptive edge detection. *2008 3rd International Symposium on Communications, Control and Signal Processing*, 1077–1081.
109. Ferzli, R., and Karam, L.J. (2009) A No-Reference Objective Image Sharpness Metric Based on the Notion of Just Noticeable Blur (JNB). *IEEE Transactions on Image Processing*, **18** (4), 717–728.
110. Marziliano, P., Dufaux, F., Winkler, S., and Ebrahimi, T. (2004) Perceptual blur and ringing metrics: application to JPEG2000. *Signal Processing: Image Communication*, **19** (2), 163–172.
111. Zhai, G., and Min, X. (2020) Perceptual image quality assessment: a survey. *Sci. China Inf. Sci.*, **63** (11), 211301.
112. Shahid, M., Rossholm, A., Lövström, B., and Zepernick, H.-J. (2014) No-reference image and video quality assessment: a classification and review of recent approaches. *J Image Video Proc*, **2014** (1), 40.
113. Ayesha, S., Hanif, M.K., and Talib, R. (2020) Overview and comparative study of dimensionality reduction techniques for high dimensional data. *Information Fusion*, **59**, 44–58.
114. Zhang, K., Wang, Z., and Liu, L. (2021) Finding Clusters and Patterns in Big Data Applications: State-of-the-Art Methods in Clustering Environments. *2021 The 5th International Conference on Compute and Data Analysis*, 8–12.
115. Solorio-Fernández, S., Carrasco-Ochoa, J.A., and Martínez-Trinidad, J.Fco. (2020) A review of unsupervised feature selection methods. *Artif Intell Rev*, **53** (2), 907–948.
116. F. T. Liu, K. M. Ting, and Z. -H. Zhou (2008) Isolation Forest. *2008 Eighth IEEE International Conference on Data Mining*, 413–422.
117. Verma, M., Srivastava, M., Chack, N., Diswar, A.K., and Gupta, N. (2012) A Comparative Study of Various Clustering Algorithms in Data Mining. *International Journal of Engineering Research and Applications (IJERA)*, **2** (3), 1379–1384.
118. Manikandan, K., Visalakshi, R., and Ponnusamy, R. (2016) Literature Survey of Data Mining Clustering Algorithms. *South Asian Journal of Research in Engineering Science and Technology*, **1** (2), 310–313.
119. Li, C., Guo, C., Ren, W., Cong, R., Hou, J., Kwong, S., and Tao, D. (2020) An Underwater Image Enhancement Benchmark Dataset and Beyond. *IEEE Trans. on Image Process.*, **29**, 4376–4389.